PEOPLE'S DEMOCRATIC REPUBLIC OF ALGERIA

MINISTRY OF HIGHER EDUCATION AND SCIENTIFIC RESEARCH

LAARBI TEBESSI UNIVERSITY OF TEBESSA

FACULTY OF EXACT SCIENCES AND THE SCIENCES OF NATURE AND LIFE

DEPARTMENT OF MATTER SCIENCES

قسم المادة

THESIS of MASTER

Specialty: **Physics of materials**

Effect of Sn doping on optical and electrical properties of CuO thin films deposited by spray pyrolysis technique

Presented by:

BOUTIGHANE Nour El Houda

Members of jury:

President	**Prof. Mohamad Lotfi BENKHEDIR**	Univ. Tebessa
Supervisor	**Dr. Labidi HERISSI**	Univ. Tebessa
Examiner	**Dr. Faouzi HANINI**	Univ. Tebessa

University season: **2024/2025**

Scanné avec CamScanner

الجمهورية الجزائرية الديمقراطية الشعبية
PEOPLE'S DEMOCRATIC REPUBLIC OF ALGERIA
وزارة التعليم العالي و البحث العلمي
MINISTRY OF HIGHER EDUCATION AND SCIENTIFIC RESEARCH
جامعة الشهيد الشيخ العربي التبسي
ECHAHID CHEIKH LARBI TEBESSI UNIVERSITY, TEBESSA
كلية العلوم الدقيقة وعلوم الطبيعة والحياة
FACULTY OF EXACT SCIENCES, NATURAL AND LIFE SCIENCES

Département : sciences de la matière

Filière : physique

Spécialité : physique des matériaux.

Année universitaire : 2024/2025.

Formulaire de levée de réserves après soutenance d'un mémoire de master

Données d'identification du candidats (es) :

Nom et prénom du candidats (es) : **Nour El Houda BOUTIGHANE.**

Intitulé du sujet : **Effect of Sn doping on optical and electrical properties of CuO thin films deposited by spray pyrolysis technique.**

Données d'identification du membre de jury :

Nom et prénom : **Mohamad Lotfi BENKHEDIR**

Grade : **Professeur**

Lieu d'exercice : **Université Echahid Cheikh Larbi Tébessi – Tébessa**

Vu le procès-verbal de soutenance de la thèse sus citée comportant les réserves suivantes :

RAS

Et après constatation des modifications et corrections suivantes :

RAS

Le : 01/07/2025

Président de jury de soutenance

الجمهورية الجزائرية الديمقراطية الشعبية
PEOPLE'S DEMOCRATIC REPUBLIC OF ALGERIA
وزارة التعليم العالي و البحث العلمي
MINISTRY OF HIGHER EDUCATION AND SCIENTIFIC RESEARCH
جامعة الشهيد الشيخ العربي التبسي
ECHAHID CHEIKH LARBI TEBESSI UNIVERSITY, TEBESSA
كلية العلوم الدقيقة وعلوم الطبيعة والحياة
FACULTY OF EXACT SCIENCES, NATURAL AND LIFE SCIENCES

Déclaration sur l'honneur de non-plagiat

(A joindre obligatoirement au mémoire, remplie et signée).

Je soussigné (e) :

Nom, Prénom : BOUTIGHANE Nour El Houda.

Régulièrement inscrit(e): en master au département : Sciences de la matière

N° de carte d'étudiant : UNI202034014958

BOUTIGHANE Nour El Houda

Année universitaire : 2024/2025

Domaine : Sciences de la matière

Filière : physique

Spécialité : Physique des matériaux

Intitulé du mémoire :

Effect of Sn doping on optical and electrical properties of CuO thin films deposited by spray pyrolysis technique

Atteste que mon mémoire est un travail original et que toutes les source utilisées ont été indiquées dans leur totalité je certifie également que je n'ai ni recopié ni utilisé des idées ou des formulations tirées d'un ouvrage article ou mémoire en version imprimée ou électronique sans mentionner précisément leur origine et que les citation intégrales sont signalées entre guillemets

Sanctions en cas de plagiat prouvé

L'étudiant sera convoqué de vent le conseil de discipline les sanctions prévues selon la gravité de plagiat sont :

- L'annulation de mémoire avec possibilité de la refaire sur un sujet diffèrent
- L'exclusion d'une année du master
- L'exclusion définitive

Fait à Tébessa, le 01/07/2025

Signature de l'étudiant (e) :

BOUTIGHANE Nour El Houda

Scanné avec CamScanner

PEOPLE'S DEMOCRATIC REPUBLIC OF ALGERIA

MINISTRY OF HIGHER EDUCATION AND SCIENTIFIC RESEARCH

LAARBI TEBESSI UNIVERSITY OF TEBESSA

FACULTY OF EXACT SCIENCES AND THE SCIENCES OF NATURE AND LIFE

DEPARTMENT OF MATTER SCIENCES

THESIS of MASTER

Specialty: **Physics of materials**

Effect of Sn doping on optical and electrical properties of CuO thin films deposited by spray pyrolysis technique

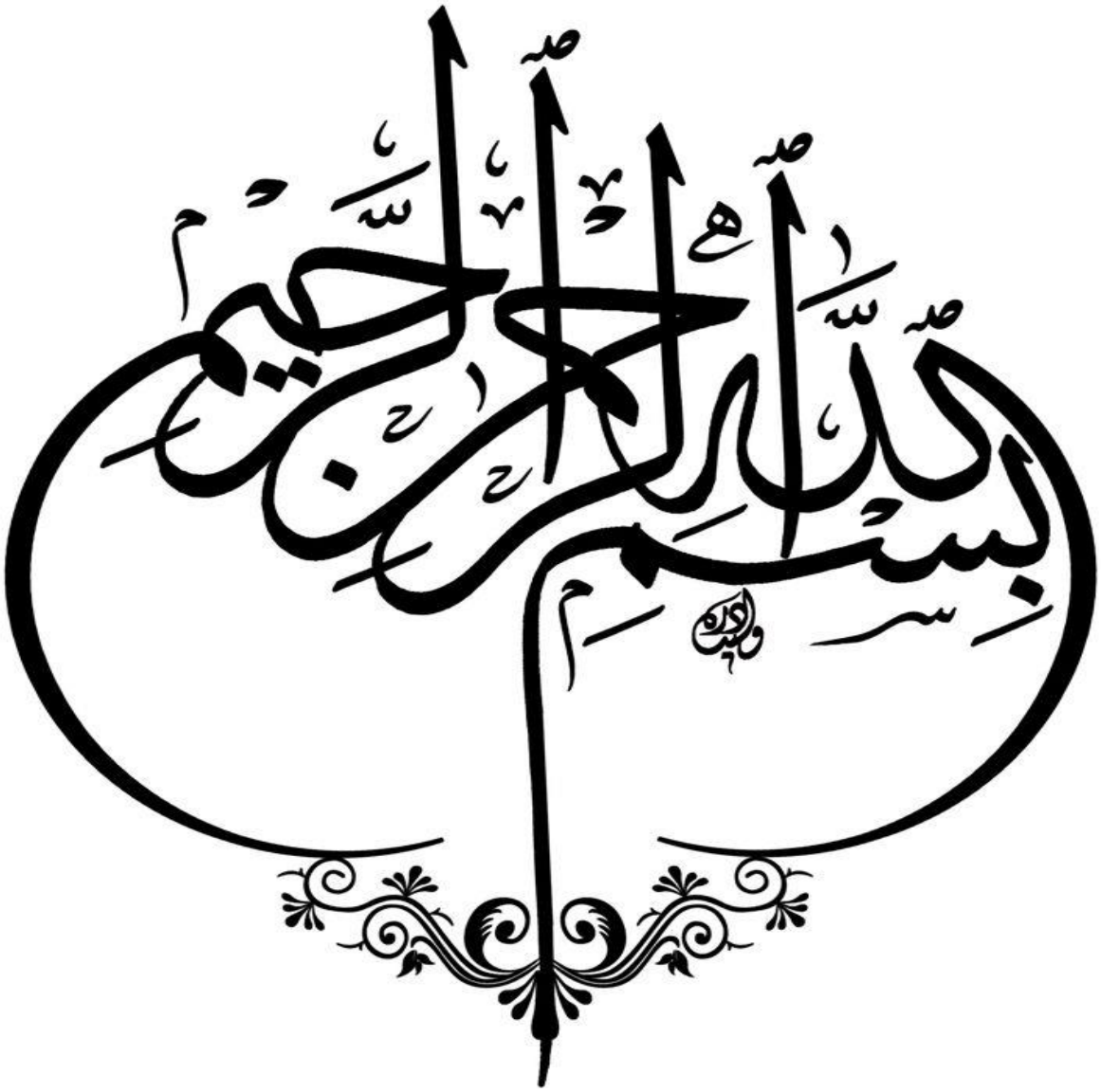
Presented by:

BOUTIGHANE Nour El Houda

Members of jury:

President	**Prof. Mohamad Lotfi BENKHEDIR**	Univ. Tebessa
Supervisor	**Dr. Labidi HERISSI**	Univ. Tebessa
Examiner	**Dr. Faouzi HANINI**	Univ. Tebessa

University season: **2024/2025**



«يَرْفَعِ اللَّهُ الَّذِينَ آمَنُوا مِنكُمْ وَالَّذِينَ أُوتُوا الْعِلْمَ دَرَجَاتٍ»

المجادلة – الآية 11

ACKNOWLEDGEMENTS

First of all, I would like to thank Allah «Exalted is he above all» who helped me fulfill this research work

I would like to express our sincere appreciation to my respectable supervisor ***Dr. Labidi HERISSI*** for his understanding and compassion, whose contribution to this work considerably added to our modest experience.

I wish to thank ***Prof. Mohamad Lotfi BENKHEDIR*** and ***Dr. Faouzi HANINI*** for agreeing to serve on my committee and who were more than generous with their expertise and precious time.

I would like to acknowledge and thank my school division for allowing me to conduct my research and providing any assistance requested.

Special thanks go to the members of the Laboratory of Materials and Structures of Electromechanical Systems and their Reliability at university Larbi Ben M'hidi of Oum-El-Bouaghi.

Finally, I would like to thank the beginning teachers, mentor-teachers and administrators in our university division that assisted me with this project. Their excitement and willingness to provide feedback made the completion of this research an enjoyable experience.

DEDICATION

I dedicate my dissertation work to my family and many friends.

A special feeling of gratitude to my loving parents, *my father* ***Abd el Fateh*** « **May God have mercy on him** » and *my mother* ***Hamza Latifa***, whose words of encouragement and push for tenacity ring in my ears.

My dear brothers and sisters « ***Hafsa, Oubaid Allah, El-Houcine***, and I give a special thanks to my wonderful sister ***Zaineb*** who has never left my side all times. »

My grandfathers, grandmothers, uncles, aunts and cousins, Especially my uncle ***Hamza Mourad*** who always supports me in times of hardship

I also dedicate this dissertation to my many friends who have supported me throughout my education life. I will always appreciate all they have done for helping and being there for me

All of you have been my best cheerleaders

BOUTIGHANE NOUR EL HOUDA

TABLE OF CONTENTS

Title	Page
List of figures	I
List of tables	III
List of symbols	IV
List of abbreviations	V
General introduction	01
Chapter I: Generalities about Cu_xO and SnO_2 thin films	03
I.1.Overview on thin film	03
I.1.1. Thin film concept	03
I.1.2. Thin film applications	03
I.1.3. Mechanism of thin films formation	04
I.1.4. Classification of thin film deposition techniques	04
I.1.4.1. Physical deposition techniques	05
I.1.4.1.1. Vacuum evaporation	05
a. Joule heating	05
b. Pulsed laser deposition	06
c. Electron beam heating	07
d. Ion Beam Assisted Deposition	08
I.1.4.1.2. Sputtering technique	08
I.1.4.2. Chemical deposition techniques	09
I.1.4.2.1. Chemical Deposition in Vapor phase	09
I.1.4.2.2. Chemical deposition in solution phase	10
A. Sol–Gel process	10
B. Electrodeposition process	11
C. Spray pyrolysis technique	12

Table of contents

I.2. Metal oxides	13
I.2.1. Definition	13
I.2.2. Types of metal oxides	13
A) n-type and p-type metal oxides	13
B) Simple and complex metal oxides	14
I.2.3. Application of metal oxides	14
I.3. Transparent conductive oxides (TCO)	15
I.4. Properties and applications of copper oxide and tin oxide	15
I.4.1. Copper oxide (Cu_xO)	15
I.4.1.1. Cuprous oxide (Cu_2O)	16
I.4.1.1.1. Crystallographic properties of Cu_2O	16
I.4.1.1.2. Optical properties of Cu_2O	17
I.4.1.1.3. Electrical properties of Cu_2O	17
I.4.1.2. Cupric oxide (CuO)	17
I.4.1.2.1. Crystallographic and physical properties of CuO	17
I.4.1.2.2. Optical properties of CuO	18
I.4.1.2.3. Electrical properties of CuO	19
I.4.2. Tin dioxide (SnO_2)	19
Chapter II : Characterization techniques of thin films	21
Part one : Elaboration of Sn-doped CuO thin films	21
II.1. Choice of ultrasonic spray pyrolysis technique	21
II.2. The decomposition of the precursor solution droplets	21
II.3. Experimental procedure	22
II.4. Experimental setup	22
II.5. Growth process details	24
II.5.1. Substrate preparation	24
II.5.2. Preparation of deposition solutions	26

Table of contents

II.5.2.1. Preparation the solution of copper (II) chloride dihydrate	26
II.5.2.2. Preparation the solution of tin (II) chloride dihydrate	27
II.5.2.3. Preparation the solution of precursor	28
II.5.2.4. Thin film deposition procedure	29
II.6. Annealing procedure of deposited samples	30
Part two: Characterization techniques of thin films	32
II.1. Optical characterization of thin films	32
II.1.1. UV-Visible-NIR spectroscopy	32
II.1.1.1. Determination of film thickness and refractive index	34
II.1.1.2. Determination of absorption coefficient	34
II.1.1.3. Determination of optical band gap	34
II.1.1.4. Determination of Urbach Energy	35
II.2. Electrical characterization	36
Chapter III: Results and discussion	38
III.1. Photos of the samples.	38
III.2. Effect of Sn-doping and annealing on the optical transmittance of CuO samples	39
III.3. Film growth kinetics	44
III.3.1. The effect of doping and annealing on the thickness of CuO:Sn	44
III.4. Optical characterizations	45
III.4.1. The effect of doping and annealing on the refractive index of CuO:Sn	45
III.4.2. The effect of doping and annealing on the Urbach energy of CuO:Sn	47
III.4.3. The effect of doping and annealing on the optical band gap of CuO:Sn	48
III.5. The effect of doping and annealing on the electrical conductivity of CuO:Sn	51
General conclusion	53
References	54

List of figures

List of figures

Figure No.	Title	Page
I.1	Schematic of thin film deposited on a substrate	03
I.2	Schematic of the different thin film deposition techniques.	05
I.3	Shows the experimental set up of Joule heating	06
I.4	PLD system setup	07
I.5	shows the experimental set up of electron beam evaporation method	07
I.6	Ion Beam Assisted Deposition	08
I.7	Schematic diagram of the sputtering technique	09
I.8	Schematic of the CVD process	10
I.9	The basic sol-gel reaction	11
I.10	Schema of Sol-Gel process	11
I.11	Electrodeposition process to deposit thin films	12
1.12	Schematic diagram of spray pyrolysis deposition	13
I.13	Crystallographic structure of copper oxide Cu_2O, in gray: copper atoms and in red: oxygen atoms	16
I.14	Crystallographic structure of CuO, in gray: copper atoms and in red: oxygen atoms	18
I.15	Geometry of tin dioxide	19
II.1	The different processes of decomposition of the spray with the increase of the substrate temperature	22
II.2	Schematic diagram of ultrasonic spray pyrolysis	23
II.3	Glass slide cutting using a diamond-tipped pen for substrate preparation.	24
II.4	substrate preparation steps.	25
II.5	Preparation of copper (II) chloride dihydrate.	26
II.6	Preparation of tin (II) chloride dihydrate.	27
II.7	Preparation the precursor solution.	28
II.8	Sn-Doped CuO solutions at different ratios.	29
II.9	Experimental setup for ultrasonic spray pyrolysis technique	30
II.10	Solution-Specific Syringes.	30
II.11	Annealing of Thin Films on electrical resistance.	31
II.12	Transmittance of light through a sample	32
II.13	The principle of operation of UV-visible spectrophotometer	33
II.14	Experimental device for UV-Vis-NIR spectroscopy	33
II.15	Fitting the measured transmittance spectra to Swanepoel's method.	34
II.16	Explanation of band gap energy.	35
II.17	Determination of Urbach energy of the film.	36
II.18	Diagram representing the principle of the four points method	36
II.19	Jandel RM3-AR Multi-position 4 Point Wafer Probe	37

List of figures

III.1	Variation of optical transmittance of CuO:Sn samples deposited on glass substrates as a function of wavelength for different doping percentages; **(a)**: before annealing, and **(b)**: after annealing.	**39**
III.2	Variation of optical transmittance of Cu_xO: Sn thin films as a function of wavelength for different Sn concentration values; **(a)**: before annealing, and **(b)**: after annealing.	**40**
III.3	Variation of optical transmittance of glass as a function of wavelength before and after annealing.	**42**
III.4	Variation of optical transmittance of Cu_xO thin films doped by 3 *at*. %, 12 *at*. % of Sn as a function of wavelength before and after annealing.	**43**
III.5	Variation of optical transmittance of SnO_2 as a function of wavelength before and after annealing.	**43**
III.6	Variation of the average thickness before and after annealing of CuO:Sn as a function of the different doping percentages.	**44**
III.7	Variation of the refractive index of thin films before and after annealing of CuO:Sn as a function of doping percentage.	**45**
III.8	Variation of thickness and refractive index of thin films before and after annealing of Cu_xO: Sn as a function of doping percentage.	**46**
III.9	Variation of the Urbach energy of thin films before and after annealing of CuO:Sn as a function of doping percentage.	**47**
III.10	Variation of optical transmittance of Cu_xO and SnO_2 of thin films before annealing as a function of wavelength.	**48**
III.11	Variation of the optical gap energy of CuO:Sn thin films before and after annealing as a function of doping percentage.	**49**
III.12	Variation of the optical band gap and Urbach energy of thin films before and after annealing of Cu_xO:Sn as a function of doping percentage.	**50**
III.13	Variation of electrical conductivity (σ) of Cu_xO:Sn thin films before and after annealing as a function of Sn concentration.	**51**

List of tables

List of tables

Table No.	Title	Page
I.1	Classification of metal oxides	14
I.2	The main crystallographic and physical characteristics of cuprite Cu_2O	16
I.3	The main crystallographic and physical characteristics of Tenorite CuO	18
II.1	Some physical properties of copper (II) chloride dihydrate	26
II.2	Some physical properties of TCD	27
III.1	Photographs of Cu_xO: Sn thin films deposited onto glass substrates.	38

List of symbols

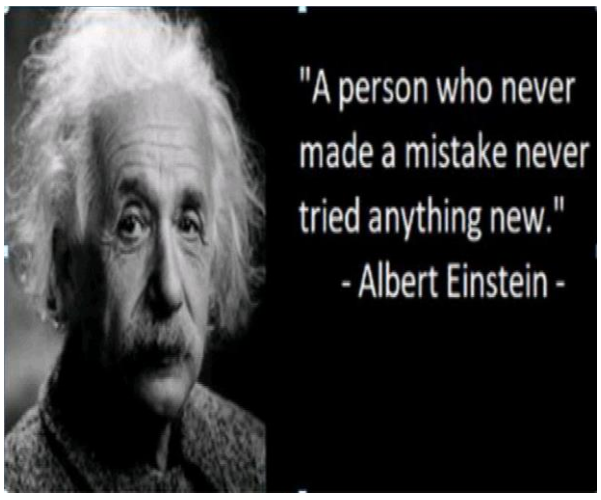
List of symbols

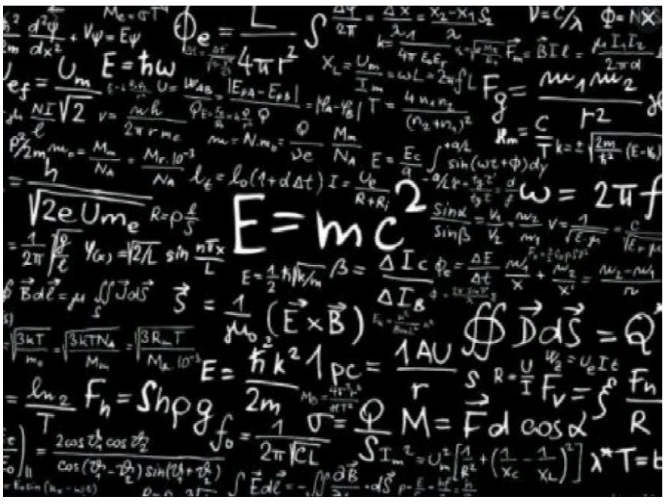
Symbol	Signification	Unit
M	Mass molar	g/mol
C	Solution concentration	mol/l
$\boldsymbol{m}$	Mass	g
V	Volume	l
$\mathbf{T}$	Temperature	℃
λ	Wavelength of incident photon	nm
$\boldsymbol{\alpha}$	Absorption coefficient	cm^{-1}
$\mathbf{T_S}$	substrate temperature	℃
$\boldsymbol{t_D}$	deposition time	min
$\emptyset$	solution flow rate	ml/h
$\boldsymbol{V_{CCD}}$	Volume of copper (II) chloride dihydrate	ml
$\boldsymbol{V_{TCD}}$	Volume of tin (II) chloride dihydrate	
$\mathbf{T_a}$	annealing temperature	℃
$\boldsymbol{t_R}$	Annealing time	min
$\mathbf{I}$	transmitted light	
$\mathbf{I_0}$	the incident light intensity	
$\boldsymbol{d}$	sample thickness	m
$\boldsymbol{T}$	Optical transmittance	%
$\boldsymbol{E_g}$	The band gap energy	eV
$\boldsymbol{h\nu}$	the photon energy	
$\boldsymbol{E_{Urb}}$	Urbach energy	
$\boldsymbol{I}$	constant current	A
$\boldsymbol{V}$	voltage	V
$\boldsymbol{R_s}$	The surface resistance	Ω
$\boldsymbol{\sigma}$	the electrical conductivity	$\Omega^{-1}cm^{-1}$
$\boldsymbol{p}$	the carrier concentration	$cm^2V^{-1}s^{-1}$
$\boldsymbol{q}$	the electronic charge	C
μ_p	the mobility of charge carriers	$cm^2V^{-1}s^{-1}$
$\mathbf{d}$	Distance	m
n	Refractive index	

List of abbreviation

Cu_2O	Copper (I) oxide or cuprite
CuO	Copper (II) oxide or Cupric
SnO_2	Tin dioxide
$Cu_xO:Sn$	Tin doped copper oxide
PVD	Physical vapor deposition
PLD	Pulsed-laser deposition
$IBAD$	Ion Beam Assisted Deposition
DC	direct current
RF	radio frequency
CVD	Chemical vapor deposition
$Sol-Gel$	Solution-gelling
(M)	metallic
(O)	oxygen
TCO	transparent conducting oxides
(CB)	conduction band
(V_{cu})	copper vacancies
$PECVD$	Plasma Enhanced Chemical Vapor Deposition
MRI	magnetic resonance imaging
$CuCl_2 \cdot 2H_2O$	copper (II) chloride dihydrate
$SnCl_2 \cdot 2H_2O$	tin (II) chloride dihydrate
CCD	copper (II) chloride dihydrate
TCD	tin (II) chloride dihydrate
$UV-VIS-NIR$	Ultraviolet-visible-near infrared

General introduction





General introduction

A large part of recent materials science research has focused on metal oxides, which are remarkable materials in many fields due to their unique electrical and optical properties [1].

Metal oxides are often wide band gap semiconductors and are commonly divided into two groups: n-type (electron-conductive type) and p-type (hole-conductive type). Metal oxides are prized for being eco-friendly, naturally abundant, easy to process, and low-cost [1,2]. However, they are normally very unstable due to their ease of oxygen exchange with the ambient atmosphere [2,3].

The growing use of thin films is directly related to their structural design, which in recent years has undergone impressive enhancement for greater performance and extended application areas. This was made possible with the development of advanced deposition systems with the ability to deliver material of superior electrical and optical characteristics, these enhanced properties have attracted extensive research towards thin films [4].

Copper oxide is a semiconductor with two stable phases: cuprous oxide (Cu2O) with cubic and cupric oxide (CuO) with monoclinic crystal structure. Both of them possess a broad direct optical band gap, about 2.1 eV for Cu2O and 1.2 eV for CuO [4]. These band gaps make it possible to efficiently absorb visible light, and therefore copper oxides have excellent prospects to be applied in numerous applications. In addition, their non-toxicity also contributes further to their utility, especially in photocatalysis and photodegradation of organic dyes [4].

Tin dioxide (SnO_2) is an n-type wide band gap semiconductor with superior electrical conductivity and optical transmittance (TCO). SnO_2 has been receiving increasing scientific and industrial attention as a thin film in recent decades due to its superior physical properties [5].

Spray pyrolysis is a versatile technique used to fabricate dense or porous oxide films, ceramic coatings, and powders. Compared to other deposition methods, it is relatively simple and low-cost, as it does not demand expensive precursors [5].

This work is a study which focuses on:

- Undoped and doped copper oxide thin films with varying atomic contents of tin (0, 3, 6, 9, and 12 *at*. %) have been prepared using the ultrasonic spray pyrolysis process on glass substrates at 350 °C.
- The optical and electrical properties of the ultimate films were measured through UV- Vis-NIR spectrophotometry and the four-point probe technique, respectively.

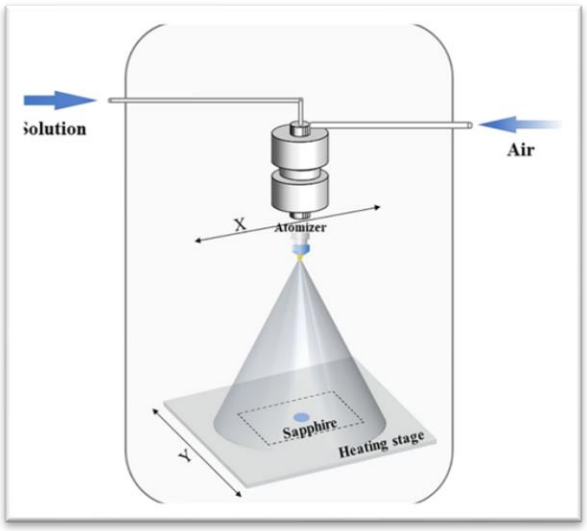
- A thorough study was conducted to investigate the influence of tin doping and annealing in air at 350 °C, on the optical and electrical characteristics of the films, in accordance with their correlation with structural and morphological modifications due to the doping and annealing processes.

The deposition and characterizations were carried out at the Laboratory of Materials and Structures of Electromechanical Systems and their Reliability (LMSSEF: *Laboratoire des matériaux et structure des systéms électromécaniques et leur fiabilité*) of Larbi Ben M'hidi University in Oum El Bouaghi.

This thesis is comprised of three main chapters, each describing a main phase of the research:

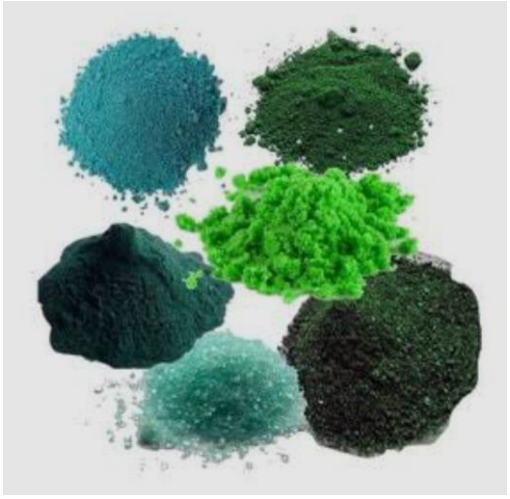
- The first chapter describes findings of bibliographic review, such as definitions and applications of thin films, deposition techniques, and a special focus on metal oxides, particularly copper oxides and tin oxide.
- The second chapter outlines the fabrication process of undoped copper oxide thin films and tin-doped (CuxO:Sn) and experimental methods employed for their electrical and optical characterization.
- The third chapter exhibits and discusses the outcomes of the experiments, such as the emergence of optical and electrical properties of copper oxide through tin doping and thermal annealing, and explores correlation between these changes.

The research concludes with an overall summary highlighting the overall stages of the research and major conclusions.



Chapter I

Generalities about copper oxide and tin dioxide thin films





Chapter I: Generalities about copper oxide and tin dioxide thin films

I.1. Overview on thin film

I.1.1. Thin film concept

A thin film is a material layer with a thickness ranging from just a few nanometers to several micrometers. Due to this extremely small thickness, which makes the film nearly two-dimensional (Figure I.1), many of its physical properties change [6,7].

During deposition, the atoms in a thin film tend to be organized in a particular pattern on the surface of a substrate aligning close to their natural crystallographic positions [6,7].

Thin films are especially useful in fields like microelectronics and integrated optics. However, their physical properties are different from that material in bulk form. A thin film is a low-dimensional structure formed through the gradual condensation of atoms, molecules, or ions [6,8].

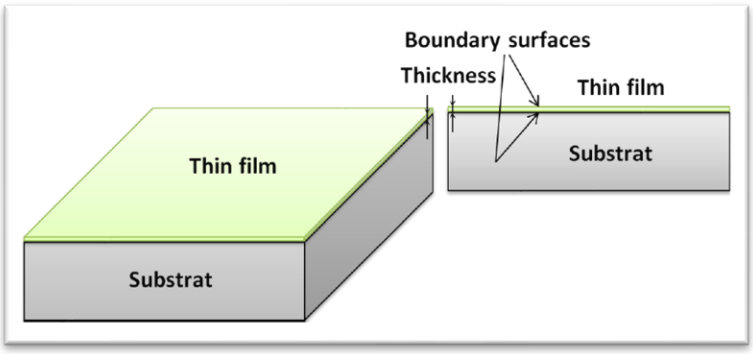


Figure I.1. Schematic of thin film deposited on a substrate [9].

I.1.2. Thin film applications

During the 20th century, more advanced applications have diversified into the following areas [2]:

- **Microelectronics:** PN junction, Transistor, Piezoelectrics material, LED lamp, Superconductor … etc.
- **Optics:** Anti-reflective layers in solar cells, Mirror staining, Anti-reflective treatment of camera lenses, Photo detection, Flat screen displays, Ophthalmic applications, optical guides …etc.
- **Mechanical:** Dry lubrication, Resistance to wear, Diffusion barriers …etc.

- **Chemistry:** Waterproof film, Gas sensor, Catalytic coatings, protective films …etc.
- **Thermal:** Thermal barrier layer.
- **Micro and nanotechnologies:** Mechanical and chemical sensors, Micro-fluidics, Actuators, Adaptive optics, Nano-photonics …etc.
- **Magnetic:** Information storage (computer memory), Security devices, Magnetics sensors …etc.
- **Decoration:** Watches, Glasses, Jewellery, Household equipment …etc.

I.1.3. Mechanism of thin films formation

Forming a thin film is challenging due to dimensional constraints that make truly two-dimensional structures impossible. These films are used in many different applications and can be made from all sorts of materials like metals, semiconductors, and insulators using various techniques. Over time, many different methods have been created to deposit thin films, and new ones are still being developed to make them more consistent and better in quality. The way a film is made plays a huge role in how it performs and that depending on the deposition technique used. Generally, the thin film formation process involves three fundamental steps [6,10]:

- The source material is first prepared in its atomic, molecular, or very fine particulate form.
- This material is then transported to the sutface of the substrate, often as a vapor, solid stream, or spray.
- Finally, the material settles on the surface and starts to grow into a thin film.

I.1.4. Classification of thin film deposition techniques

The deposition ways of the thin films are different from one another. It refers to the diversity of the domain where we use these films [8]. The thin film deposition methods may be divided into two categories based on how material transport and film deposition which it shown in Figure I.2 [11,12]: (i) physical methods (PVD) and (ii) chemical methods.

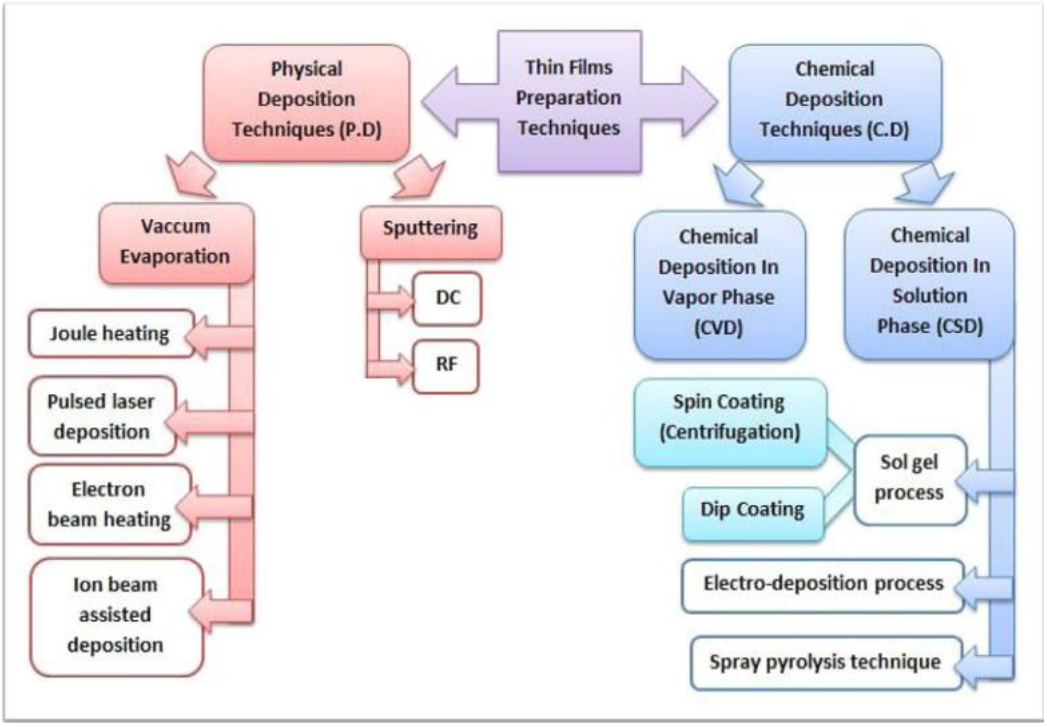


Figure I.2. Schematic of the different thin film deposition techniques.

I.1.4.1. Physical deposition techniques

In physical methods or Physical Vapor Deposition (PVD), the pure source material is gasified via physical processes like thermal evaporation or by bombardment from an energetic beam of electrons, photons or ions. There are no chemical reactions that occur in the entire process [11]. There are two types of PVD: Vacuum evaporation and Sputtering technique.

I.1.4.1.1. Vacuum evaporation

Vacuum evaporation is a simple and general deposition technique applied to the thin film deposition. the idea of the process is simply to heat a material in a vacuum chamber until it vaporizes. The vapor condenses on a substrate which is maintained at a specifc temperature [11,13].

It is applicable to all the metals except refractory metals because of their low vapor pressure. The vapor pressure of the material is raised to that necessary for evaporation or sublimation by heating the material. Different of these parameters control the quality of the deposition, which include substrate, source temperature and substrate temperature, source-substrate distance, and chamber pressure. Various techniques of heating the material can be used in this process, such as resistance wires, electron beams, and radio-frequency-heated crucibles [11].

a. Joule heating

Sources of evaporation in simple form are wires or foils made of refractory metals like molybdenum (Mo), tantalum (Ta), or tungsten (W). Due to their low electrical resistances, they need to be heated by means of a power supply with low voltage but high current, for example 0–5 V and 0–400 A (about 2 kW in alternating current), as shown in Figure I.3 [8,39].

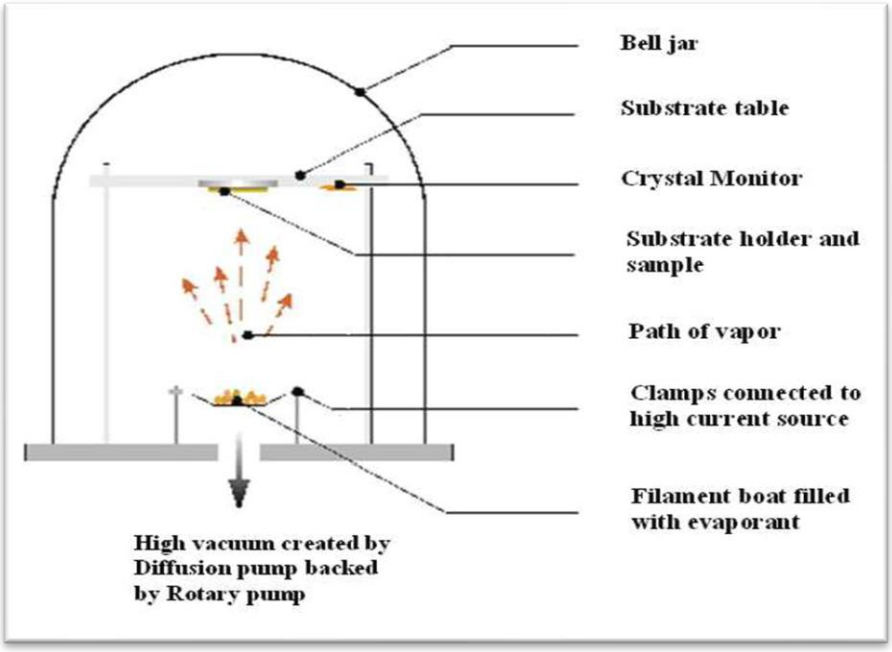


Figure I.3. Shows the experimental set up of Joule heating [14].

b. Pulsed laser deposition

Laser ablation or Pulsed Laser Deposition (PLD) is another physical deposition technique to deposit the thin film-coating system [2,15]. PLD depends on focusing a laser beam on a material in order to vaporize it and then condense the ionized particles on a substrate heated or not. These ionized particles have high kinetic energy and strike the surface at very high speeds. Figure I.4 shows the schematic diagram of PLD [2,16].

various laser sources are used to ablate the target and the most common sources are KrF (248 nm), XeCl (308 nm), and Nd-YAG laser (1064 nm). Making CuO thin film by this technique has the advantage of being able to use of high oxygen and that of making high quality crystalline films with speed of high growth even at low temperature [2,15,17,18].

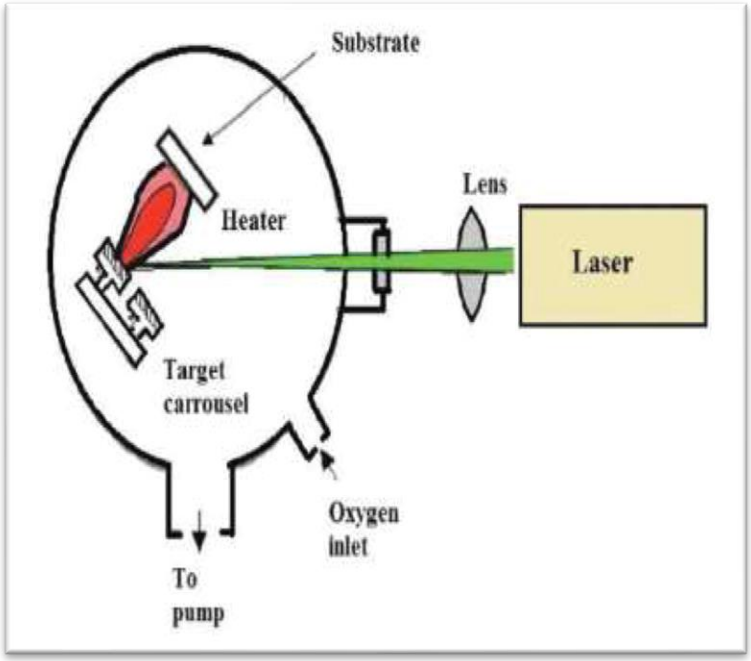


Figure I.4. Schematic of pulsed-laser deposition [2].

c. Electron beam heating

This type of evaporation is another method of physical deposition which has a different heating technique. Using a filament for the generation of intensive beam of electrons and steered through both electric and magnetic fields to hit the target in order to vaporize it under vacuum environment as shown in Figure I.5 Thin films prepared by electron beam evaporation are of good quality and purity [19,39].

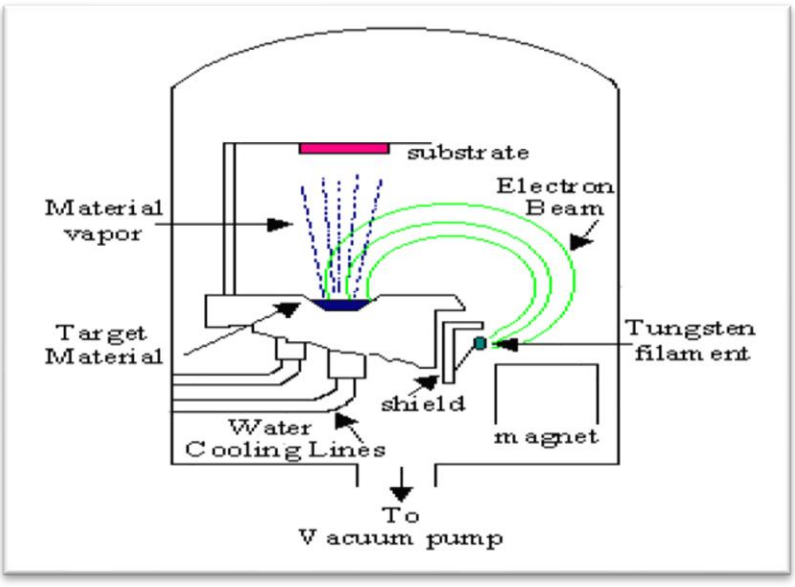


Figure I.5. Shows the experimental set up of electron beam evaporation method [14].

different materials can be prepared by electron beam evaporation technique such as amorphous and crystalline semiconductors, metals, oxides, and molecular materials [20].

d. Ion Beam Assisted Deposition

Ion Beam Assisted Deposition (IBAD) is an imporved technique for producing adherent surface coatings with specific properties. the setup for this method consists of a cylindrical vacuum chamber, a rotating cooled target holder, an electron gun with evaporation source, a duoplasmatron ion source for gaseous ions, and the necessary power supplies and controls (Figure I.6) [12,21].

Evaporation and ion bombardment can be carried out sequentially or in parallel. The ion source generates ions having energies up to 30 keV in the direction of the component surface. The component is positioned where evaporated material and ion beam intersect. For argon, the beam current to a maximum of about 7 mA [12,21].

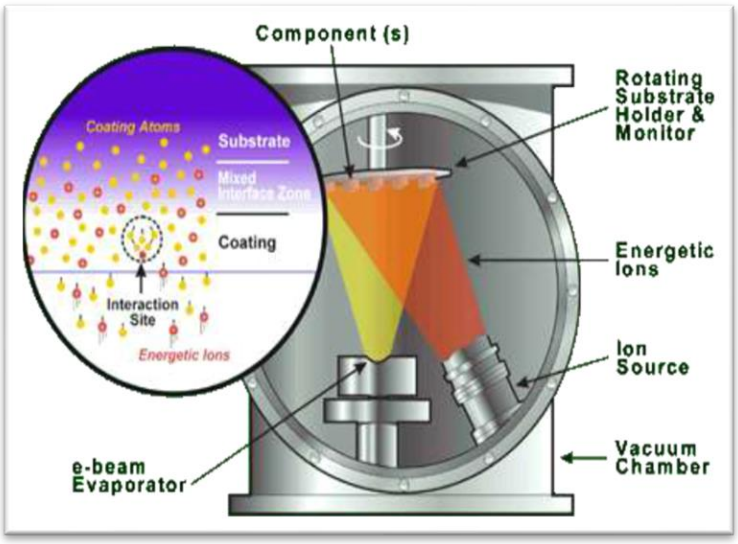


Figure I.6. Ion Beam Assisted Deposition [12].

I.1.4.1.2. Sputtering technique

In this method, the substrate is placed inside a low pressure chamber containing an inert gas (generally Argon). For the inert gas atoms to be ionized, an electric field must be applied which also causes for these ions to be accelerated by a potential difference and directed toward a cathode made of the material to be deposited (the target). Due to the impact of the accelerated ions with the target, atoms are ejected

from its surface and subsequently deposited onto the substrate. In certain cases, a reactive gas such as oxygen is introduced into the chamber in addition to argon which will create a chemical reaction with the sputtered atoms to form a compound film. This process is called reactive cathodic sputtering. It enables forming thin films of low resistivity and layers of good stoichiometry having an average transmission in the visible [22,23], which illustrate in Figure I.7.

It has several advantages, high-melting point materials can be easily formed by sputtering while having a composition similar to the composition of the starting materials in addition to it's compatibility with ultrahigh vacuum systems and reactive gases.The sputtering sources are compatible with reactive gases such as oxygen. However, it also has limitations such as thick coatings cannot be obtained and there is a difficulty to deposit uniformly on complex shapes [22,24].

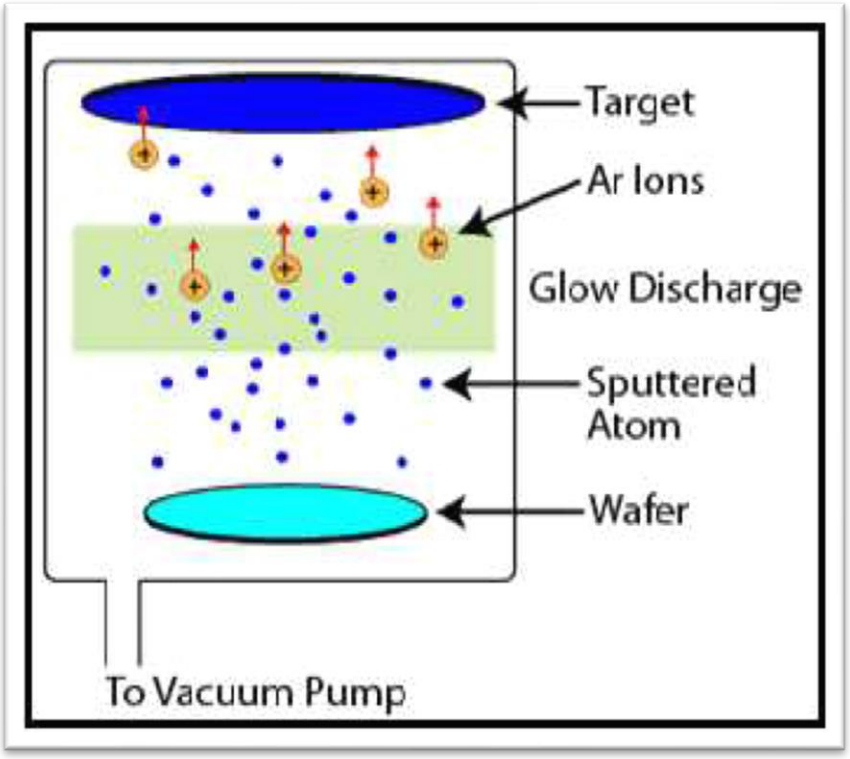


Figure I.7. Schematic diagram of the sputtering technique [8].

I.1.4.2. Chemical deposition techniques

In chemical deposition techniques, the source material is blended with a volatile precursor, usually in the state of vapor or solution that leads to a chemical reaction when they settle on the substrate surface, resulting in the formation of a thin film of the desired composition, and by products removed afterwards [11].

I.1.4.2.1. Chemical deposition in vapor phase

Chemical Vapor Deposition (CVD) is one commonly used process where thin films are deposited through chemical reactions among the precursors in the gas phase. After they are introduced to the reaction chamber, the source gases travel towards the substrate and a chemical reaction on the substrate surface takes place, leading to the deposition of a thin film. As depicted in Figure I.8, CVD entails several important steps [25].

The most crucial stages of CVD, as depicted in figure I.8, are [25]:

1. Evaporation of reagent and transport into the reactor by bulk gas flow.
2. Mass transport of reactants to the substrate surface.
3. Adsorption of reactants onto the surface, followed by surface diffusion to growth sites.
4. Surface reactions and nucleation, with growth of the film.
5. Desorption and removal of reaction byproducts from the reaction zone.

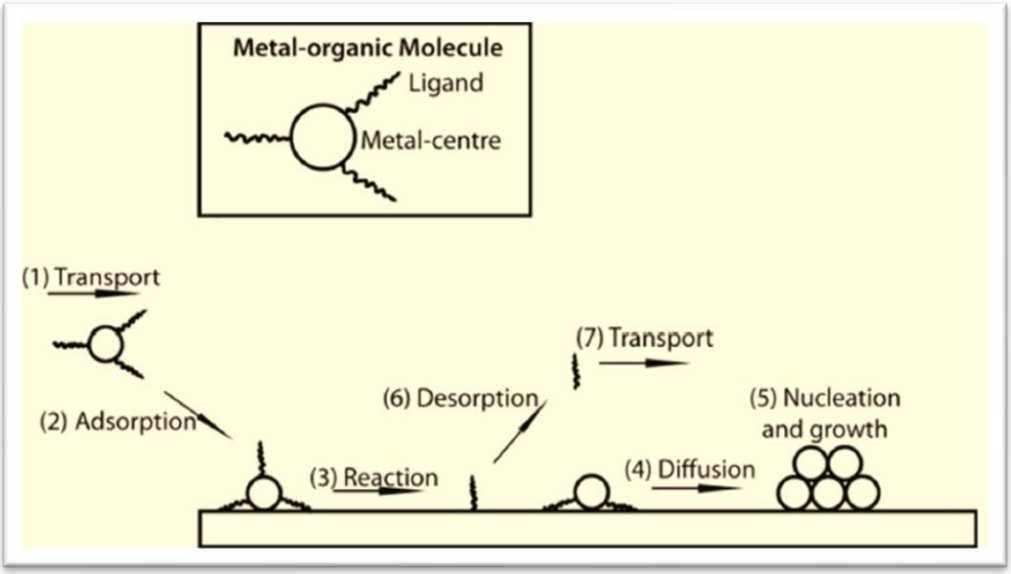


Figure I.8. Schematic of the CVD process [25].

I.1.4.2.2. Chemical deposition in solution phase

Chemical solution deposition (or CSD), is an overarching term referring to any technique where in a solution of a chemical precursor is used to deposit a film [26]. The CSD is a very flexible method as it provides good control of stoichiometry and has large areas for surface coverage. The application protocols used in CSD are

quite similar to those used in the semiconductor industry for photoresist use, a well proven high throughput method [27].

It contains many methods, including the following:

A. Sol-gel process

Sol-gel is a straightforward way to turn liquid precursors into high-purity glass, gels, or ceramic powders at room temperature. starting with a colloidal suspension (the sol) and, in a matter of minutes or hours, watch it evolve into a solid network (the gel). Once the solvent dries out, what's left is a robust, glass-like coating. The core chemistry illustrated in Figure I.9 involves two steps: first, hydrolysis creates the sol, and then condensation builds a continuous film on the substrate [12,28].

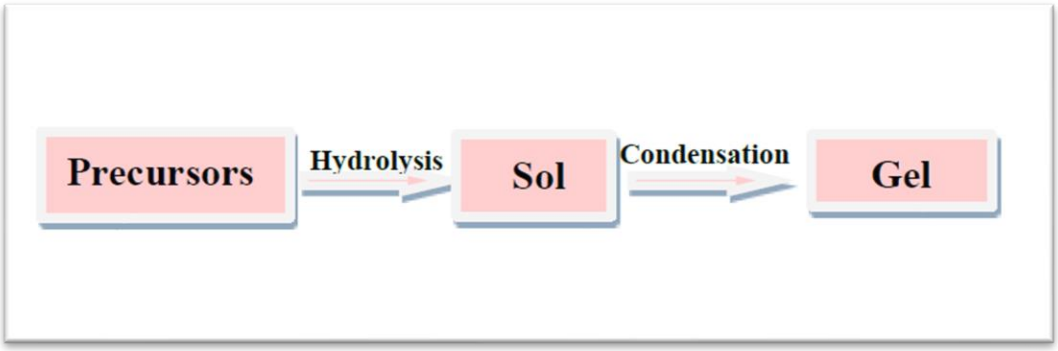


Figure I.9. The basic sol-gel reaction [12].

When it comes to applying that sol, we have two popular options (FigureI.10):

1. **Spin-coating (Centrifugation):** pour the sol onto a rapidly spinning substrate. Centrifugal force flings off the excess, and by tweaking the spin speed and run time, then dial in exactly how thick the film will be [12,29].
2. **Dip-coating:** a slower but gentler method—immerse the substrate in the solution, lift it out at a steady pace, then let it dry and finally anneal it to crystallize the layer. The withdrawal speed directly controls the deposit's thickness [12,30].

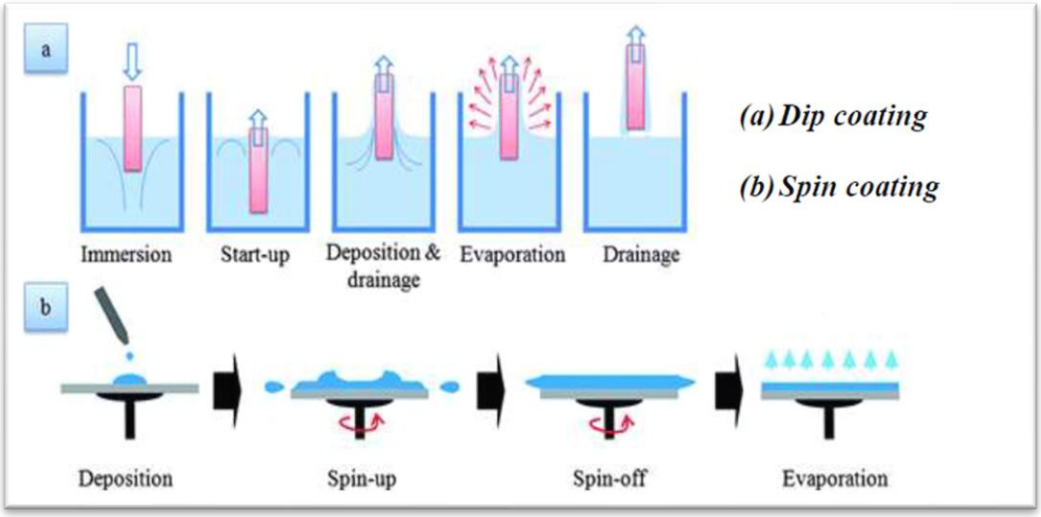


Figure I.10. Schema of Sol-Gel process [12].

B. Electrodeposition process

Electrodeposition is a non-vacuum electrochemical technique preferred for thin film deposition owing to its capacity to deposit multi-component alloys at low temperature. In this method, deposition of thin metallic films is performed on the surface by the reduction of cations without any unwanted reactions [5,31]. Figure I.11 shows the thin films electrodeposition process.

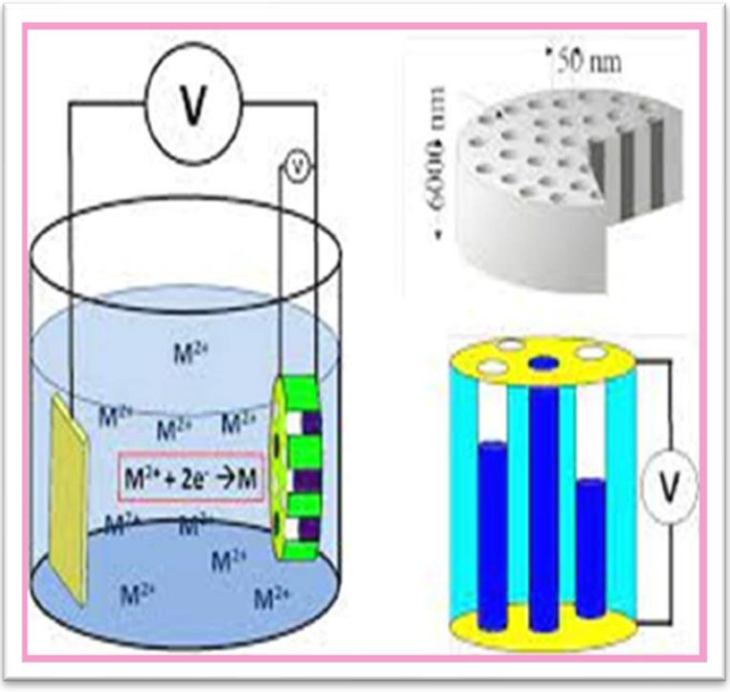


Figure I.11. Electrodeposition process to deposit thin films [5].

C. Spray pyrolysis technique

Spray pyrolysis is a deposition technique used to prepare thin and thick films. It is a very simple method that does not require high-quality chemicals. Typical spray pyrolysis equipment consists of an atomizer, a precursor solution, and a substrate heated with a temperature controller. Ultrasonic atomizers are used in the spray pyrolysis technique. In an ultrasonic atomizer, ultrasonic frequencies (around 40 kHz) produce the short waves required for fine atomization [32].

The deposition of thin films using the spray pyrolysis technique involves spraying a solution of a metal salt onto a heated substrate (Figure I.12). The droplets arriving on the substrate lead to the formation of a deposit after decomposition and a chemical reaction on the surface [32].

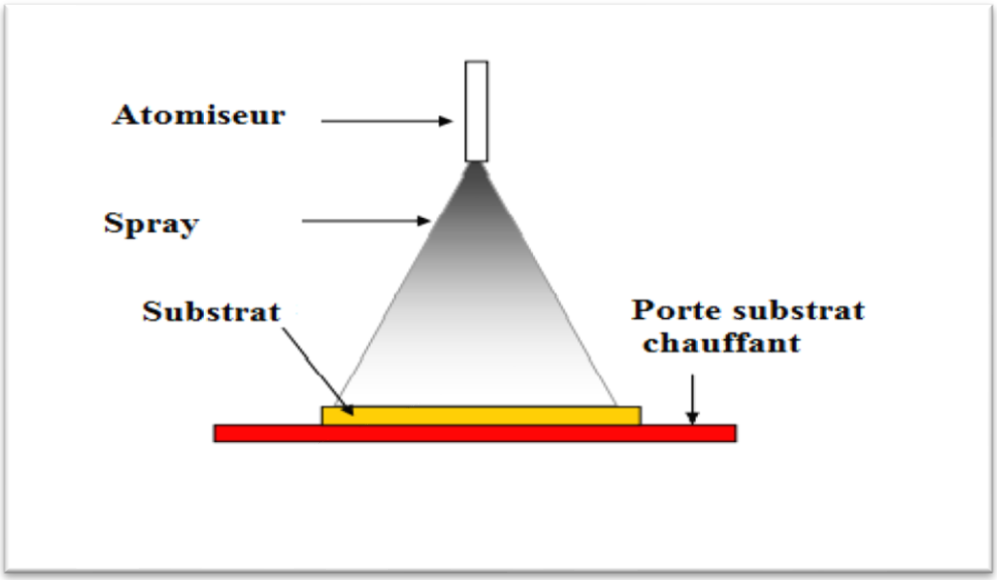


Figure I.12. Schematic diagram of spray pyrolysis deposition [32-34].

I.2. Metal oxides

I.2.1. Definition

Metal oxides (MO) are homogeneous solid phases containing one or more types of metal cations in different oxidation states ($M1_xM2_yO_z$), where M is the chemical symbol of the metal atom and O that of oxygen. Among the notable metal oxides are Al_2O_3, ZnO, Cr_2O_3, CuO, Fe_2O_3, SnO_2, and $BaTiO_3$ [2,35,36].

Metal oxides are categorized by either their type of conductivity (electron or hole) or by whether they are single or complex [2,37].

I.2.2. Types of metal oxides

A) n-type and p-type metal oxides

There are two main families of metal oxides (Table I.1):

1. **P-type:** Conduction by holes, relatively unstable due to easy oxygen exchange with air, but employed in high-temperature oxygen sensors [2,38].
2. **N-type:** Conduction by electrons, more stable and fulfilling the majority of gas-sensor applications [2,35,38].

Table I.1. Classification of metal oxides [2].

n-type Metal oxide	p-type Metal oxide
SnO_2	CuO
WO_3	NiO
ZnO	La_2O_3
TiO_2	Ag_2O
In_2O_3	TeO_2
Ta_2O_5	$BaTiO_3$

B) Simple and complex metal oxides

Metal oxides can be classified into two main categories:

1. **Simple metal oxides:** comprise a metal such as SnO_2, TiO_2, SiO_2, … [39].
2. **Mixed metal oxides:** composed of two or more components such as $BaTiO_3$ that have slightly or very different properties corresponding simple oxides [2,38].

A particularly Notable property is the production of very acidic sites linked to the interface or to the bond between the two components [38].

I.2.3. Application of metal oxides

Metal oxides have a variety of applications that are directly linked to their physical and chemical properties. These applications cover a wide range of technological fields, including microelectronics, the photovoltaic industry, gas

sensors, anti-corrosion coatings, paints (e.g: ZnO and TiO_2), biotechnology, photocatalysis and nanotechnology. In nanotechnology, nanostructured metal oxides represent an ever-evolving area of research. They contribute to the miniaturisation of the systems in which they are integrated, and it is impossible to list them all systems [33].

The properties of metal oxides are closely linked to the elaboration methods and the preparation and deposition techniques, parameters and conditions. Mastery of these techniques and parameters enables us to produce metal oxides with well- defined physicochemical properties. To obtain nanostructural properties, it is necessary to control several parameters, such as the size, shape, composition and degree of agglomeration of the nanoparticles, which can take different forms [33].

When obtained in a finely divided state, oxide crystallites must exhibit the following characteristics in particular [33]:

- A well-defined chemical composition.
- Uniform size.
- Morphology adapted to applications.

Like all nanomaterials, metal oxide nanostructures are made up of nano-objects that can take many different forms, including monoliths, powders, particles, fibres, tubes, thin films and structural constituents [33].

I.3. Transparent conductive oxides (TCO)

There is a family of oxides that are transparent and can become n-type conductors if they have an excess of electrons in their lattice. This excess can be created by structural defects that induce an imbalance in the oxide's stoichiometry or by appropriate doping. These oxides are known as transparent conductive oxides (TCOs). TCOs have a high band gap and are, in fact, degenerate semiconductors; that is to say, their Fermi level is very close to the conduction band (CB), or even within this band in the case of heavily doped TCOs. This means that the CB is already well filled with electrons at room temperature, making TCOs conductive. Furthermore, the high band gap of TCOs (~3–4 eV) prevents them from absorbing photons with energies below this gap, rendering them transparent to visible light [23].

The main TCOs used as transparent electrodes for solar cells have long been SnO2 and ITO. Since the 1980s, a third TCO, zinc oxide (ZnO), has been increasingly used for these applications. This thesis focuses on the latter TCO [23].

I.4. Properties and applications of copper oxide and tin oxide

I.4.1. Copper oxide (Cu_xO)

Copper has two principal oxides, cuprite (Cu_2O) and Tenorite (CuO) corresponding to oxidation state I and II, respectively [40].

These materials have some interesting properties making them useful in a wide range of applications such as solar cells, catalysis, superconductors, magnetic storage, gas detection, photothermal conversion and photoconductive materials. On the nanoscale, the modifications in their electronic structure fundamentally alter their native, predominantly because of the quantum confinement effects [41].

I.4.1.1. Cuprous oxide (Cu_2O)

I.4.1.1.1. Crystallographic properties of Cu_2O

Copper (I) oxide or cuprite crystallizes in the space group Pn3m. the oxygen ions form a body-centered cubic lattice, while the cuprous ions occupy the centers of half of the edge-sharing cubes with side length a/2 (Figure I.13). The highly symmetric crystal structure of cuprous oxide Cu_2O (cubic structure) consists of Cu^+ ions located at the (¼, ¼, ¼) positions of the conventional FCC unit cell and O^{2-} ions positioned at the (¾, ¾, ¾) sites of the BCC lattice [40].

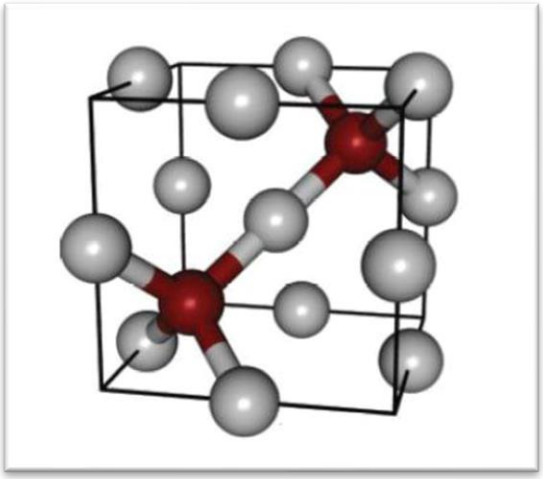


Figure I.13. Crystallographic structure of copper oxide Cu_2O, in gray: copper atoms and in red: oxygen atoms [40].

The crystal structure features copper atoms in a linear coordination with two oxygen atoms, creating a 3D framework of O-Cu-O dumbbells. The key crystallographic properties of Cu_2O are outlined in the table I.2 [40]:

Table I.2. The main crystallographic and physical characteristics of cuprite Cu_2O [40].

Structure	Cubic
Space Group	Pn_3m
Lantern Parameter (Å)	a=b=c=4.2696
Lantern Volume ($Å^3$)	77.83
Cu-O Bond Length (Å)	1.849
Density (g/cm^3)	6.106

I.4.1.1.2. Optical properties of Cu_2O

Cuprous oxide (Cu2O) is a semi-conductor with a bulk material band gap of 2.13 eV, such that thin films of it permit yellow light (λ >580nm). Its band gap varies in thin-film systems. Wavelengths below (<580nm) are strongly absorbed: blue light is completely prevented from passing, while green light is partially permitted to pass. This differential absorption gives Cu2O films their characteristic yellow-transparent appearance.

Due to its partial visible-light transparency and p-type character, Cu_2O is an interesting material for transparent conductive oxides (TCOs). Work today is mainly focused on its optoelectronic applications, such as transparent photovolataics and diodes, where it is utilized to exploit its transparent p-n junction function [40].

I.4.1.1.3. Electrical properties of Cu_2O

The hole density and conductivity of Cu_2O are influenced to a great extent by copper vacancies (V_{Cu}), which are acceptors. Studies show that conductivity is improved at high temperatures due to higher hole density (Young et al.). Annealing enhances conductivity and mobility in nanocrystalline Cu_2O (Gopalakrishna et al.).

In addition, Cu_2O nanotubes possess a high mobility (>95 cm2 V-1 s-1), which allows tunable electrical properties through stoichiometry and crystallinity control during deposition (Liao et al.) [40].

I.4.1.2. Cupric oxide (CuO)

I.4.1.2.1. Crystallographic and physical properties of CuO

CuO crystalliezs in a monoclinic system belonging to the C2/c space group. In this structure, every copper atom is surrounded by four oxygen atoms arranged in a rectangular geometry, whereas each oxygen atom is coordinated by four copper atoms forming a distorted tetrahedral configuration [40] (Figure I.14).

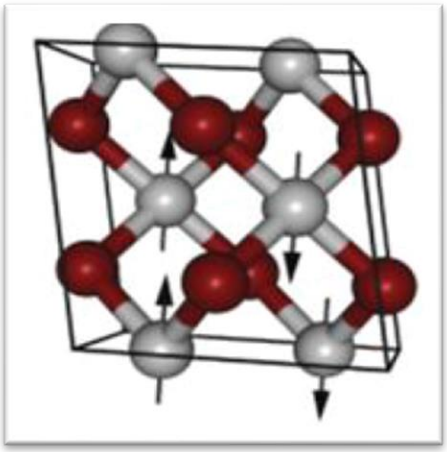


Figure I.14. Crystallographic structure of CuO, in gray: copper atoms and in red: oxygen atoms [40].

CuO is an intrinsic p-type semi-conductor and is anti-ferromagnetic, possessing a local magnetic moment of 0.60 μB per unit cell. Although its properties resemble those of high-Tc superconducting cuprates, CuO contains only Cu-O bonds. The table I.3 summarizes key crystallographic and physical properties of CuO [40].

Table I.3. The main crystallographic and physical characteristics of Tenorite CuO [42].

Structure	Monoclinic
Space Group	C2/c
Lantern Parameter (Å)	a=4.69 b=3.42 c=5.13
Lantern Volume ($Å^3$)	81.12
Cu-O Bond Length (Å)	1.96
Density (g/cm^3)	6.51

I.4.1.2.2. Optical properties of CuO

CuO is classified as a p-type semi-conductor because of acceptor levels arising from copper vacancies. Its band gap ranges from 1 to 2 eV, influenced by synthesis

techniques [26,33,43]. Nevertheless, experimental confirmation of the precise band gap value and its direct/indirect transition nature remains uncertain. The thin-film refractive index and absorption coefficient of CuO depend on processing conditions, with the refractive index varying from 1.9 to 3 based on the deposition on the deposition approach [40].

I.4.1.2.3. Electrical properties of CuO

CuO is usually described as a p-type semiconductor with relatively low electrical conductivity. It's also antiferromagnetic, and its local magnetic moment has been measured at about 0.60 μB. Reported values of resistivity vary quite a bit, in fact, they've ranged from as low as 1.0 Ω·cm to as high as 10^7 Ω·cm, mostly depending on how the material was prepared [40].

Thin films made using methods like spray pyrolysis or PECVD tend to have much lower resistivity, typically around 10 Ω·cm and between 0.5 and 5 Ω·cm. These relatively low values are often thought to result from things like deviations from stoichiometry or electrical conduction happening along grain boundaries. It's also possible that this behavior is linked to the material's low level of impurities and its thermal stability when processed in low oxygen environments [40].

I.4.2. Tin dioxide (SnO_2)

Tin dioxide (SnO_2) is an inorganic compound primarily found in the mineral cassiterite. This colorless solid is commonly regarded as an oxygen-deficient n-type semi-conductor [12,44]. SnO_2 crystallizes in a tetragonal structure with lattice parameters a = b = 4.738 Å and c = 3.186 Å (Figure I.15). The unit cell has six atoms, four oxygen (O) atoms and two tin (Sn) atoms. There are three tin atoms coordinated to each oxygen atom, and six oxygen atoms octahedrally coordinating each tin atom [12,45].

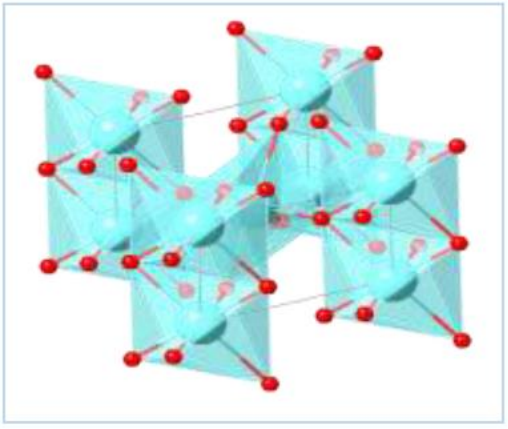
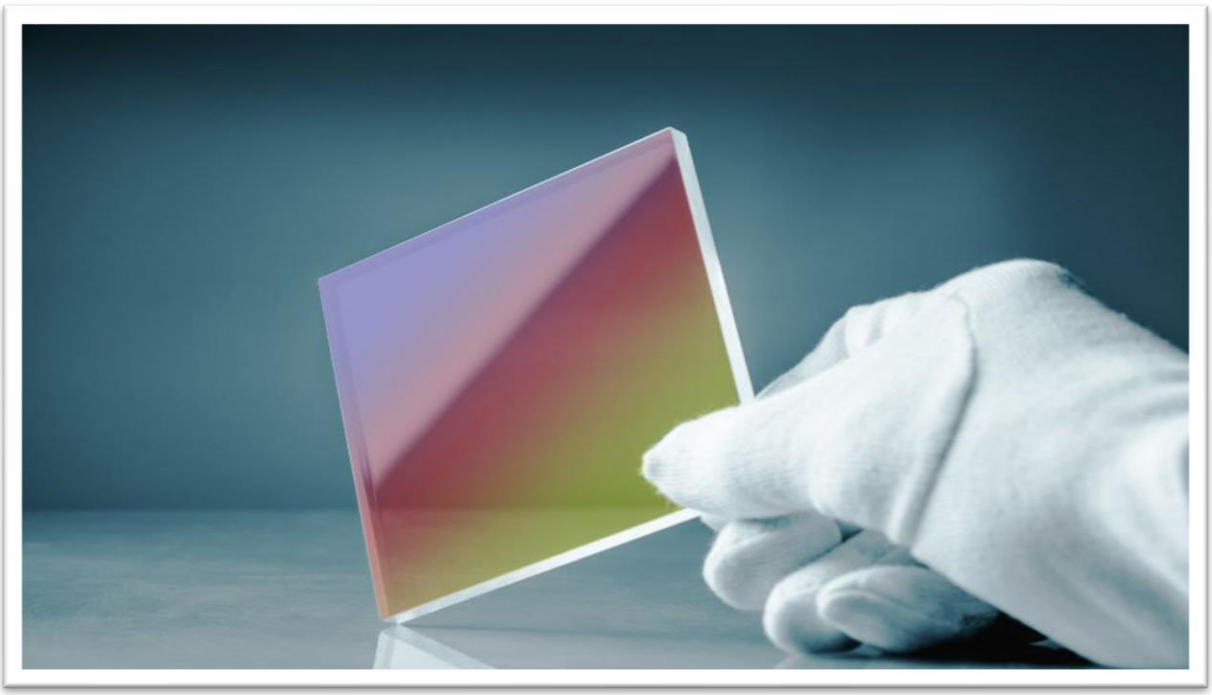


Figure I.15. Geometry of tin dioxide

Even though SnO_2 is insoluble in water, it dissolves in acidic and basic solutions. Metal reduction followed by burning of the tin air is used in tin dioxide purification industrially [12,44].

According to its unique features, SnO_2 has some technological uses, such as [5,46]:

- Its application of its magnetic nature in nanonparticles in magnetic data storage and magnetic resonance imaging (MRI).
- Use as catalytic materials, energy-conserving coatings and anti-static coatings.
- Utilization as anti-reflection coatings and electrodes in photovoltaic devices.



Chapter II

Characterization techniques of thin films



Chapter II: Characterization techniques of thin films

To determine the structural, electrical and optical properties as well as the thickness of thin films, various analytical methods were employed as described below [8]:

Part one: Elaboration of Sn-doped CuO thin films

II.1. Choice of ultrasonic spray pyrolysis technique

Ultrasonic spray pyrolysis is an efficient and applicable aerosol-based method for the fabrication of nanoparticles and the deposition of thin films. Its key advantages are [5,22]:

- ✓ Safety and stability: The process is non-combustible and non-explosive and essentially inert to the human body.
- ✓ Ease of use: It is easy to install and quick and allows one to have precise control over the chemical content of the deposited material.
- ✓ Versatility in doping: Multiple precursors can be used at the same time and doping processes become efficient.
- ✓ Good-quality films: The film created is of higher uniformity and structural stability.
- ✓ Cost-effectiveness: It is economical and scalable and can be applied in industrial processes.
- ✓ Large-area deposition: The technique is very useful for application in applications having uniform coating of large areas, such as solar cells and flat-panel displays.

II.2. The decomposition of the precursor solution droplets

The droplet decomposition mechanism varies with substrate temperature. Spitz and Viguié [47] identified four distinct processes (Figure II.1):

- ➢ Process A (Low Temp.): Droplets impact the substrate, spread and decompose post-solvent evaporation.
- ➢ Process B (Intermediate Temp.): Solvent evaporates mid-flight; dry precipitates decompose/react on the substrate without gas-phase intermediates.
- ➢ Process C (High Temp.): Solvent evaporates before deposition, forming vapors thet adsorb diffuse and react on the substrate (CVD-like mechanism).
- ➢ Process D (Very high Temp.): Vapor-phase nucleation generates solid particles deposited as loose films.

Films from Processes A/D exhibit porosity and weak adhesion, whereas Process C yields dense, adherent coatings—critical for thin-film performance [47].

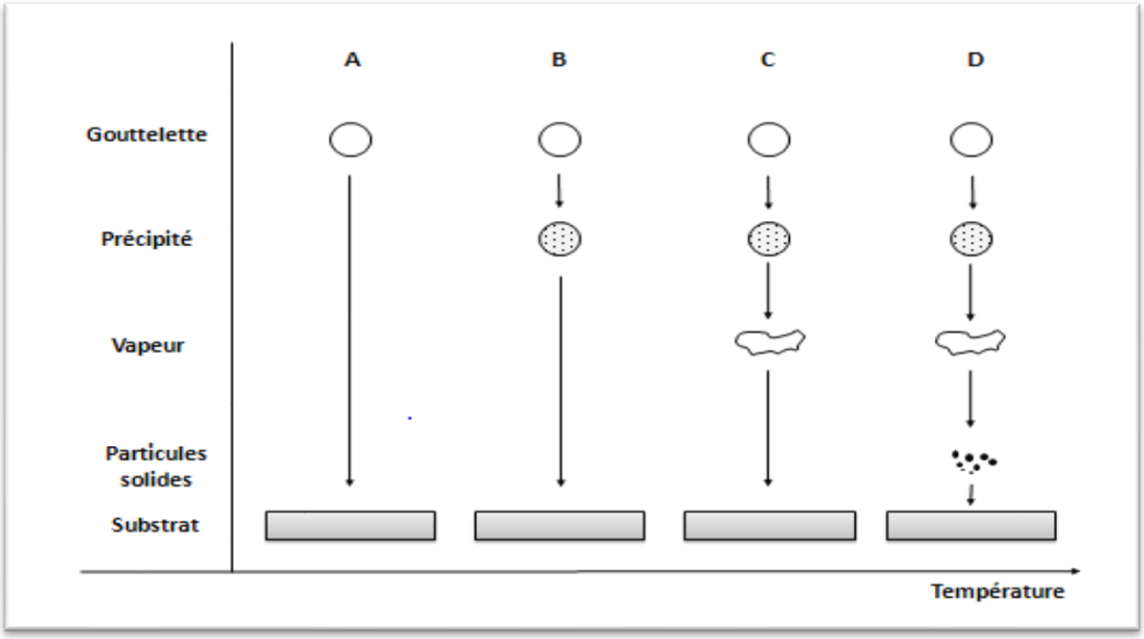


Figure II.1. The different processes of decomposition of the spray with the increase of the substrate temperature [47].

II.3. Experimental procedure

This work involves the ultrasonic spray pyrolysis deposition of tin-doped and undoped copper oxide (Cu_xO:Sn) thin films. The work discusses the influence of tin doping and annealing on optical and electrical properties of deposited films with others being constants such as substrate temperature (T_S), precursor solution concentration (C), deposition time (t_D), and solution flow rate (ϕ). The dopant solutions were prepared using ($CuCl_2 \cdot 2H_2O$) and tin (II) chloride dihydrate ($SnCl_2 \cdot 2H_2O$) dissolved in deionized water. From the knowledge of the properties of undoped and Sn-doped CuO films, the aim of this study is to explain the impact of the addition of the dopants and deposition geometry on the optical, and electronic properties of copper oxide-based thin films for potential optoelectronic applications.

II.4. Experimental setup

This experimental work was performed at the Materials and Structure of Electromechanical Systems and their Reliability Laboratory (LMSSEF*: Laboratoire des matériaux et structure des systéms électromécaniques et leur fiabilité*) of Larbi Ben M'hidi University in Oum El Bouaghi. Both undoped copper oxide (CuO) and tin-doped copper oxide (CuO:Sn) thin films were

deposited using the ultrasonic spray pyrolysis method from simple precursor solutions, as illustrated in Figure II.2.

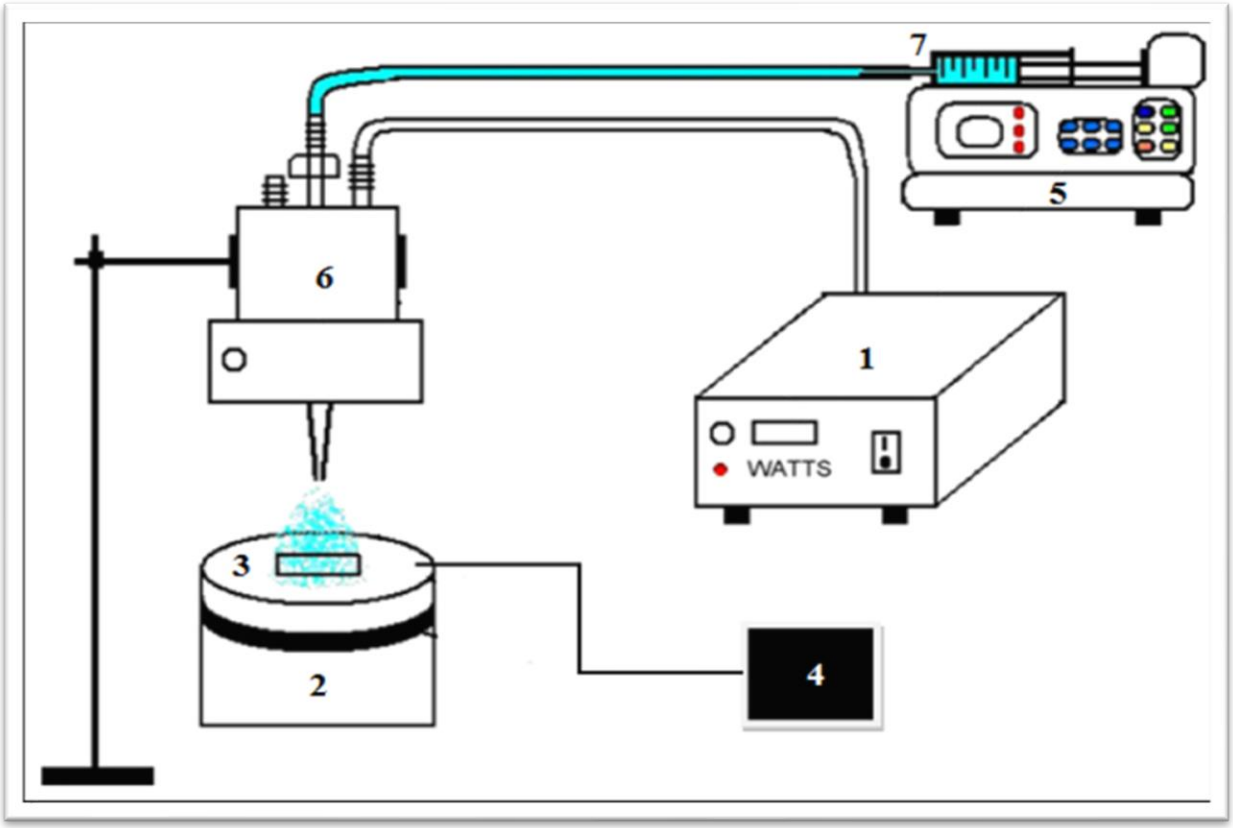


Figure II.2. Schematic diagram of ultrasonic spray pyrolysis [11].

1. **40 kHz Ultrasonic Generator:** Generates and focuses ultrasonic waves on the atomizer.

2. **Heating Resistance:** Uniformly heats the substrate**.**

3. **Substrate Holder:** Fixtures the substrate in place.

4. **Thermometer:** Gives instantaneous substrate temperature reading.

5. **Syringe Pump (PHOENIX D-CP):** Controls solution flow rate accurately.

6. **Atomizer**: Converts the solution into microscopic droplets by ultrasonic vibration.

7. **Solution Syringe**: Holds and releases the precursor solution.

II.5. Growth process details

II.5.1. Substrate preparation

The substrate significantly impacts thin film growth, as lattice and thermal mismatches with the film often induce stress. The substrate choice affects the film's crystalline quality, optical properties, and electrical performance [25].

In this work, Cu_xO:Sn thin films were deposited in a microscopy slide clear glass ground edges substrates in surface area of (25.4 x 76.2) mm^2 and (1-1.2) mm thick, where each slide was sectioned into three substrates using a diamond-tipped pen (Figure II.3).



Figure II.3. Glass slide cutting using a diamond-tipped pen for substrate preparation.

- Reasons for Choosing Glass [25]:
- ✓ Economic (low cost).
- ✓ Optical characterization (glass is transparent in the visible, suitable for optical studies).
- ✓ Minimizes stress due to similar thermal expansion coefficients of glass ($8.5 \times 10^{-6}\ K^{-1}$) and CuO ($12.5x10^{-6}K^{-1}$), Cu_2O ($2.5x10^{-6}K^{-1}$) and SnO_2 ($11.7 \times 10^{-6}\ K^{-1}$) [3].

Substrate cleaning is a significant operation in thin-film technology, performed before deposition to eliminate impurities that could have negative impacts on film properties. Cleaning involves the removal of impurities with a variety of chemical solutions (Figure II.4.a) without compromising the substrate, breaking contaminant-substrate bonds to free unwanted particles [25].

Serial cleaning of the glass slides is as follows:

1. First rinsing in distilled water (Figure II.4.b).
2. Soaking in a 5-minute bath of methanol in an ultrasonic cleaner (Figure II.4.c).
3. Second rinsing with distilled water to eliminate residual methanol (CH_3OH).
4. Soaking in acetone (5 minutes ultrasonic cleaner) to strip off lipid layers (Figure II.4.d).
5. Third and final rinse in distilled water to remove acetone.
6. Drying with Joseph paper.



Figure II.4. substrate preparation steps.

II.5.2. Preparation of deposition solutions

II.5.2.1. Preparation the solution of copper (II) chloride dihydrate

In our work, copper (II) chloride dihydrate (CCD) ($CuCl_2 \cdot 2H_2O$) with a molar mass (M_{CCD} = 170.48 g/mol) was used as a source of Cu material (Table II.1), figure II.5.a, with distilled water as the solvent. To obtain a CCD solution (V_{solC}) with a molarity of (C=0.05 M), figure II.5.b, a quantity ($m_{CCD}=C.M_{CCD}.V_{solC}$) of CCD is mixed in a volume of distilled water (V_{solC}=400 ml).

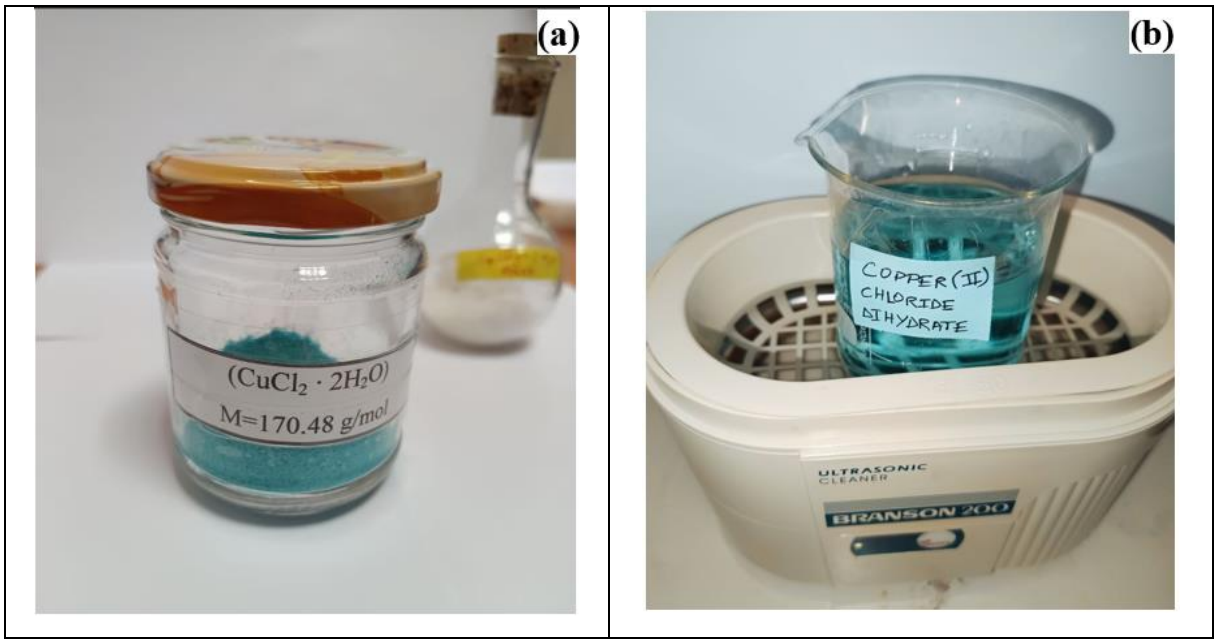


Figure II.5. Preparation of copper (II) chloride dihydrate.

Table II.1. Some physical properties of copper (II) chloride dihydrate [17].

Appearance	Crystalline solid
Molecular formula	$CuCl_2 \cdot 2H_2O$
Molar mass (g/mol)	170.48
Color	Turquoise
Density (g/cm³)	2.51
Melting point (°C)	498
Boiling point (°C)	993

II.5.2.2. Preparation the solution of tin (II) chloride dihydrate

In our work, tin (II) chloride dihydrate (TCD) ($SnCl_2 \cdot 2H_2O$) with a molar mass (M_{TCD} = 225.63 g/mol) was used as a source of Sn material (Table II.2), figure II.6.a, with distilled water as the solvent. To obtain a TCD solution (V_{solT}) with a molarity of (C=0.05 M), figure II.6.b, a quantity (m_{TCD}=C.M_{TCD}.V_{solT}) of TCD is mixed in a volume of distilled water (V_{solT}=20 ml) where, a scale was used KERN442-432N accurately± 0.001g to weigh a certain amount of CCD.

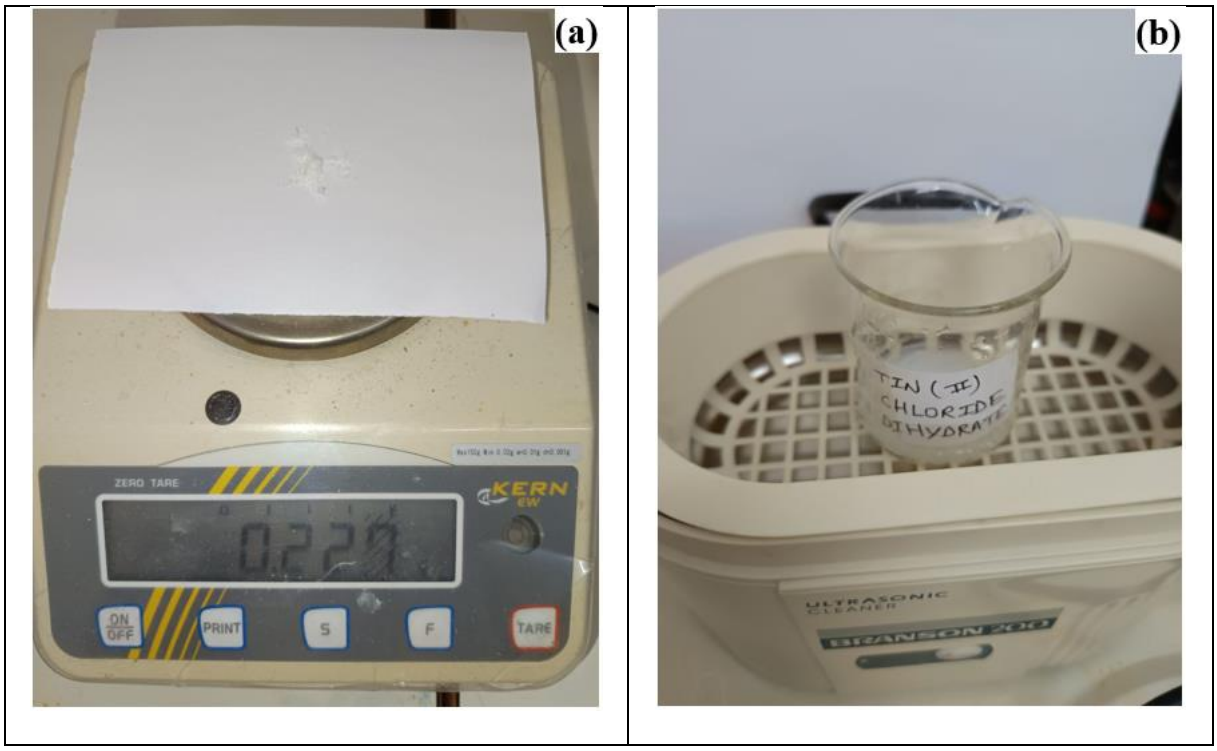


Figure II.6. Preparation of tin (II) chloride dihydrate.

Table II.2. Some physical properties of TCD [11].

Appearance	White crystalline solid
Molecular Formula	$SnCl_2 \cdot 2H_2O$
Molecular Weight (g/mol)	225.63
Density (g/cm^3)	2.71
Melting point (°C)	38
Boiling point (°C)	652

II.5.2.3. Preparation the solution of precursor

After preparing separate solutions of copper (II) chloride dihydrate and tin (II) chloride dihydrate, the two solutions were mixed in a beaker of capacity 25 ml (Figure II.7). The volumes of each solution (Figure II.8) were determined based on the doping rate (r) as follows:

- Volume of CCD solution: $V_{CCD} = (1\text{-}r) \times 25$ ml
- Volume of TCD solution: $V_{TCD} = r \times 25$ ml

The total volume of the mixture was maintained at 25 ml, satisfying the condition:

$V_{CCD} + V_{TCD} = 25$ mL

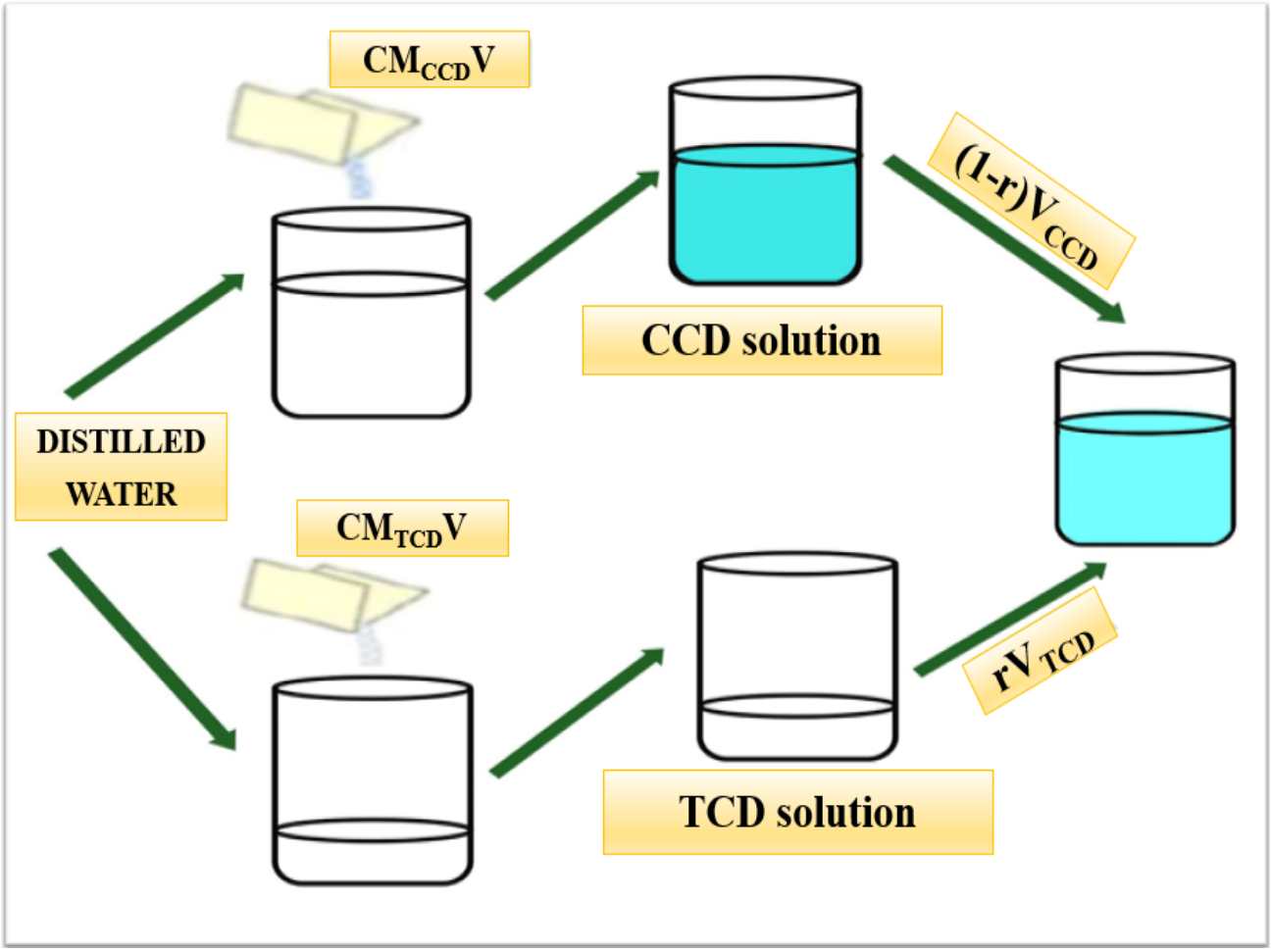


Figure II.7. Preparation the precursor solution.

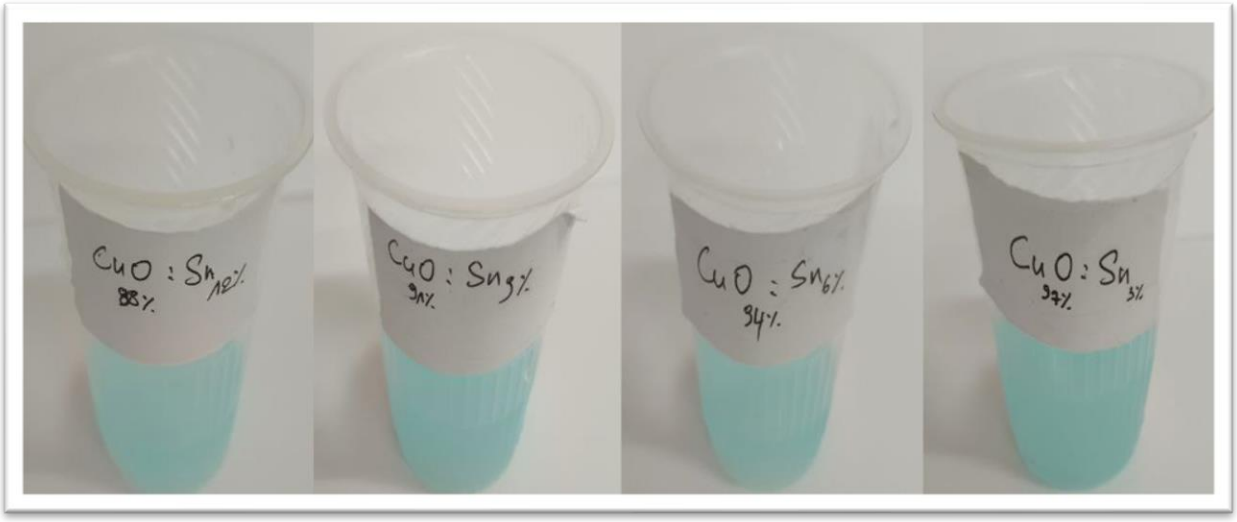


Figure II.8. Sn-Doped CuO solutions at different ratios.

II.5.2.4. Thin film deposition procedure

- **Preparation and Safety:** Pre-deposition, equipment was checked and calibrated in order to ensure the highest functioning and safety as indicated in Figure II.9.
- **Substrate Heating:** The substrate was laid on top of an electrical resistor and heated gradually from ambient temperature to deposition temperature (*Ts*= 350°C) in order to prevent thermal shock.
- **Precursor Solution Delivery:** Precursor solution was loaded in a syringe (Figure II.10) and pumped by a syringe pump at a constant flow rate of 60 ml/h along a distance of 5 cm between nozzle and substrate to facilitate controlled delivery. An ultrasonic generator was employed to atomize the solution into minute droplets getting closer to a state of vapor.
- **Cooling and Deposition:** The solution was deposited on the 4-minute preheated substrate. Heating ceased after deposition and the substrate was cooled slowly to room temperature in an attempt to prevent thermal stress and cracking. The films appeared transparent with a clear brown color and had good adhesion on the glass substrates.



Figure II.9. Experimental setup for ultrasonic spray pyrolysis technique



Figure II.10. Solution-Specific Syringes.

II.6. Annealing procedure of deposited samples

Due to the unavailability of necessary equipment, electrical resistance heating was utilized instead of a heat treating furnace (Figure II.11). The annealing technique was used on all samples (0 at. %, 3 at. %, 6 at. %, 9 at. %, and 12 at. %), where the heat treatment was performed to recrystallize the thin films and enhance their structural properties. The chosen annealing temperature (Ta=350°C) was sufficient enough to facilitate crystallization without degrading the samples.



Figure II.11. Annealing of Thin Films on electrical resistance.

The annealing was done by several procedures as follows:

- The samples (CuO:Sn) were not placed above resistor while it was hot to avoid thermal shock.
- Three samples were annealed simultaneously for 60 min Until the samples are completed (Figure II.11).
- After annealing, the heater was turned off, and the samples were left to cool slowly to preventcracking due to rapid air exposure (especially critical for thin films deposited on glass substrates).

After annealing: The color changed to dark brown, indicating a possible oxidation.

Part two: Characterization techniques of thin films

To ascertain electrical and optical properties and the thickness of thin films, various analysis methods were used as detailed below:

II.1. Optical characterization of thin films

Thin films possess unique optical behavior, which is extensively utilized in different applications. Thus, optical absorption characterization has emerged as a useful tool for the investigation of transparent samples. For instance, it is extensively applied to investigate quantum confinement effects because of the reduced size of crystallites. Parameters such as transmittance, absorption coefficient, optical band gap, Urbach energy, and refractive index can be precisely evaluated using a spectrophotometer [12].

II.1.1. UV-Visible-NIR spectroscopy

UV-Vis-NIR spectrophotometry is founded on the interaction between electromagnetic radiation and matter in the ultraviolet-visible-Near infrared ranges of spectra. The incident light intensity (I_0) and intensity of transmitted light (I) through a sample are measured by the spectrophotometer in the form of absorbance (A) and thickness of the sample (d), as shown in Figure II.12 [48].

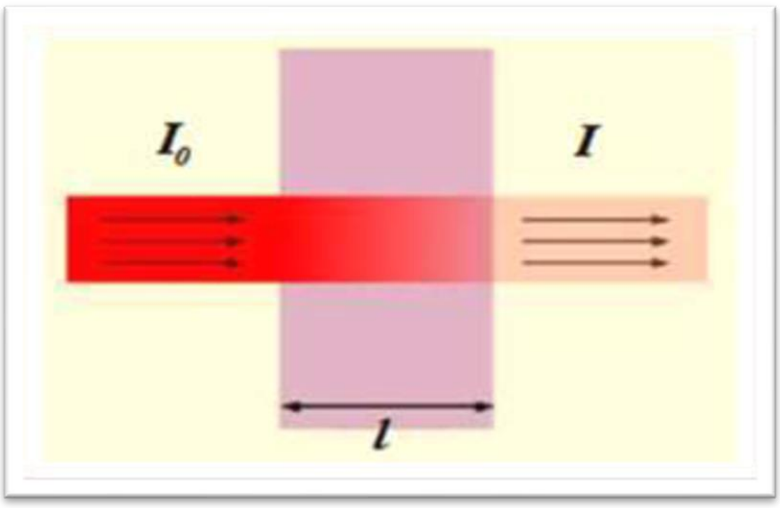


Figure II.12. Transmittance of light through a sample [48].

The spectrophotometer's dual-lamp source is a continuous spectrum across the UV-Vis-NIR wavelengths. There is separation of discrete wavelengths by a monochromator, enabling spectral scanning by mechanical adjustment. The wavelength beam selected is bounced off a

synchronizing mirror, passes through the reference and sample cells, and is examined by an amplifier that compares incident and transmitted intensities (Figure II.13) [49].

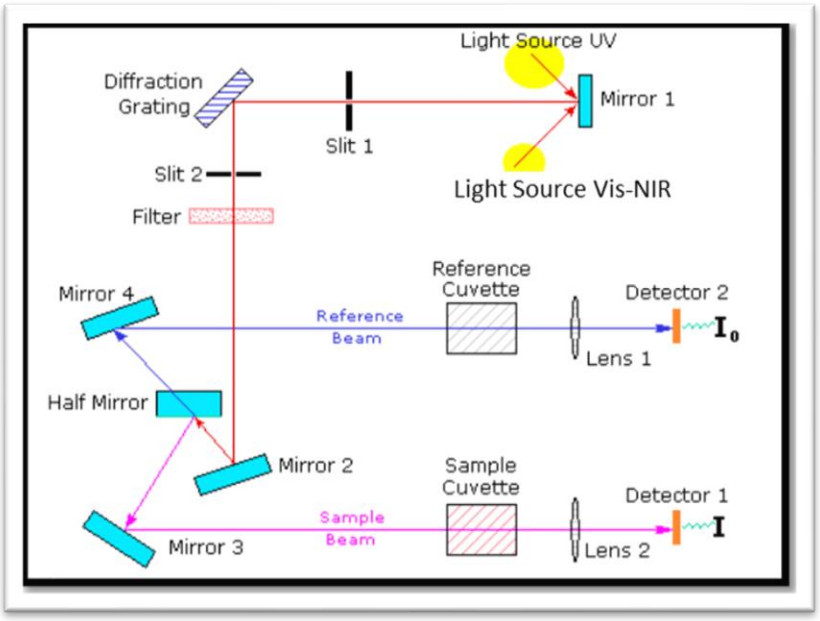


Figure II.13. The principle of operation of UV-visible spectrophotometer [12].

In this study, significant optical parameters of thin films were computed from transmittance-wavelength spectra in UV-Visible region. The readings were taken using a JASCO V-630 UV-Visible spectrophotometer with a range of 190-1100 nm, as presented in Figure II.14 [12].



Figure II.14. Experimental device for UV-Vis-NIR spectroscopy.

II.1.1.1. Determination of film thickness and refractive index

The thickness, refractive index, and optical band gap of thin films can be determined by analyzing their transmission spectra (T). The transparency curve is divided into two domains, each described by a wavelength-dependent function with constants including sample properties. These parameters are optimized using least squares regression to fit experimental data. For observed pairs (x_n,), the least squares method minimizes errors between simulated and measured transmission curves (FigureII.15). For Sn-doped CuO films, we extract thickness and refractive index by fitting simulated data to experimental spectra using adjustable parameters in Fit software [4].

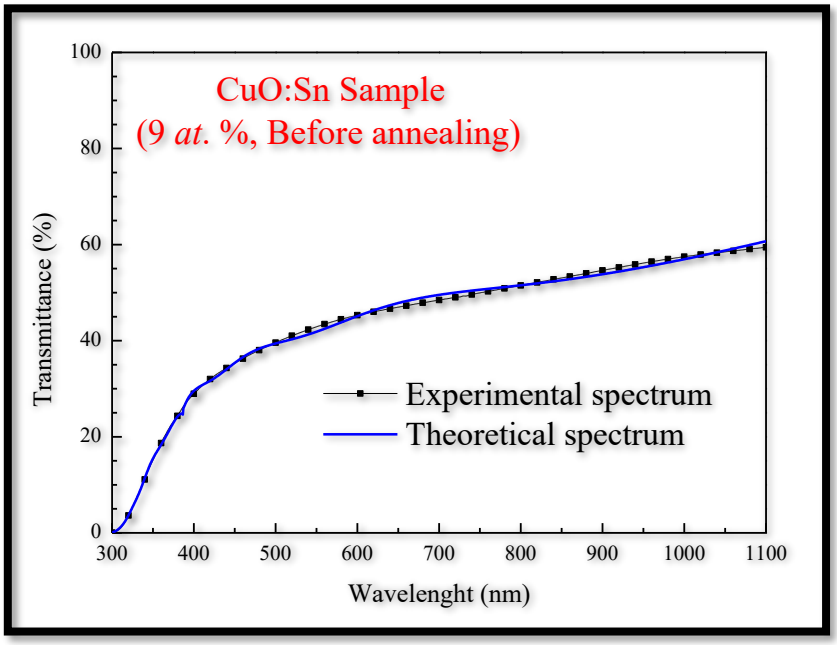


Figure II.15. Fitting the measured transmittance spectra to Swanepoel's method.

II.1.1.2. Determination of absorption coefficient

Based on transmittance spectra, we can determine the absorption coefficient (α) for the materials formed, we use the relation, which known by the beer-lambert low [8,50].

$$\alpha = \frac{1}{d} \ln \frac{1}{T} \qquad \text{(II.1)}$$

II.1.1.3. Determination of optical band gap

The band gap energy (E_g) is calculated from the Tauc plot, versus the photon energy $h\nu$ [8,51].

$$(\alpha h\nu)^2 = A(h\nu - E_g) \quad \text{(II.2)}$$

where $A\ is\ constant$.

If $(\alpha h\nu)^2$ is extrapolated to the x-axis intersection($(\alpha h\nu)^2$=0), formula (II.2) implies that the photon energy equals the band gap energy $(h\nu = E_g)$. This method is commonplace to extract band gap energies from transmission data, A diagram illustrating the band gap is shown in figure II.16.

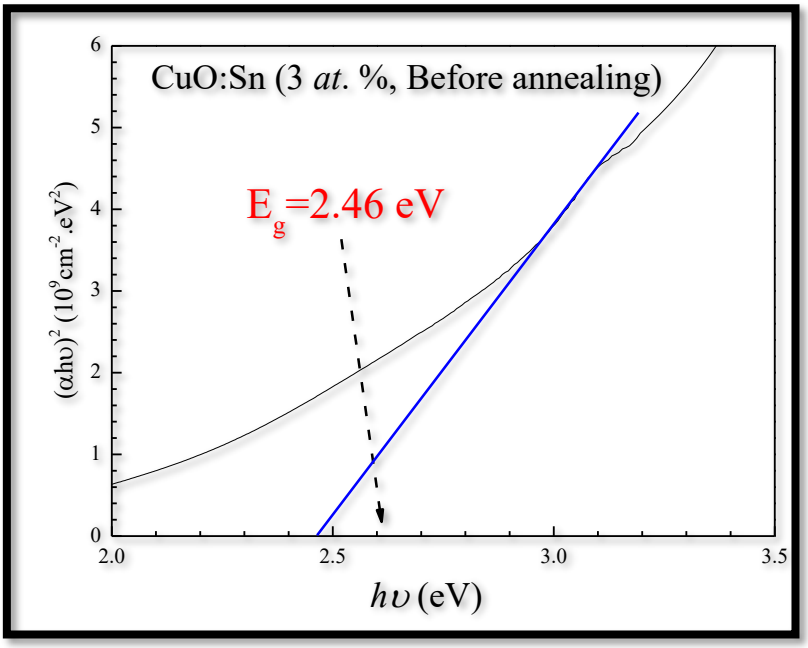


Figure II.16. Explanation of band gap energy.

II.1.1.4. Determination of Urbach Energy

Urbach energy (E_{Urb}) defined as the width of the localized states available in the optical band gap that affects the optical band gap structure and optical transitions. The Urbach tail is determined by the Urbach's relation [8,52]:

$$\alpha = \alpha_0 exp\left(\frac{h\upsilon}{E_{Urb}}\right) \quad \text{(II.3)}$$

Where α_0 is constant

It is possible to determine the value of Urbach energy (Figure II.17), through drawing a statement $ln\alpha$ as function of $h\upsilon$ based on the equation:

$$ln\,\alpha = \left(\frac{1}{E_{Urb}}\right) h\upsilon + ln\,\alpha_0 \qquad \text{(II.4)}$$

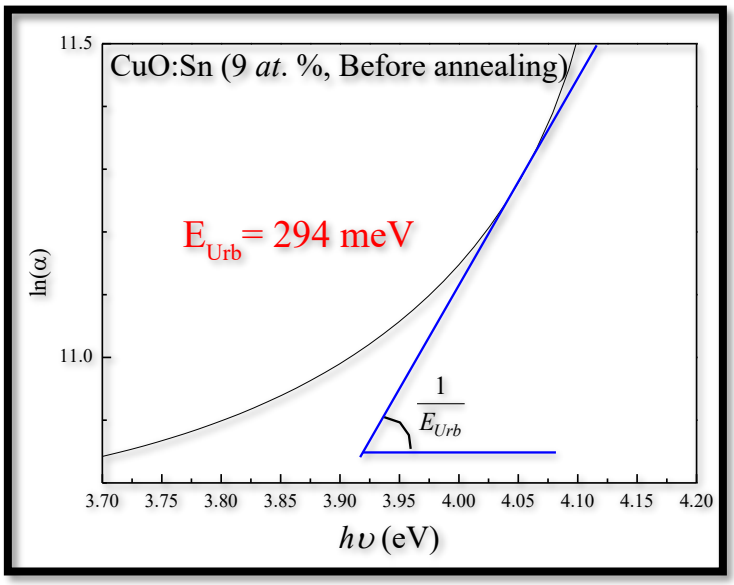


Figure II.17. Determination of Urbach energy of the film.

II.2. Electrical characterization

For the determination of the electrical conductivity of the thin films, we performed measurements using a four-point probe system (Figure II.18). The technique is founded on a probe of four linearly and equally spaced (distance a) tips grown on the sample surface. The outer two electrodes apply a current of fixed intensity (I) from a high-precision source through the film, and the two inner electrodes monitor the induced voltage (V) generated by the film resistance [48].

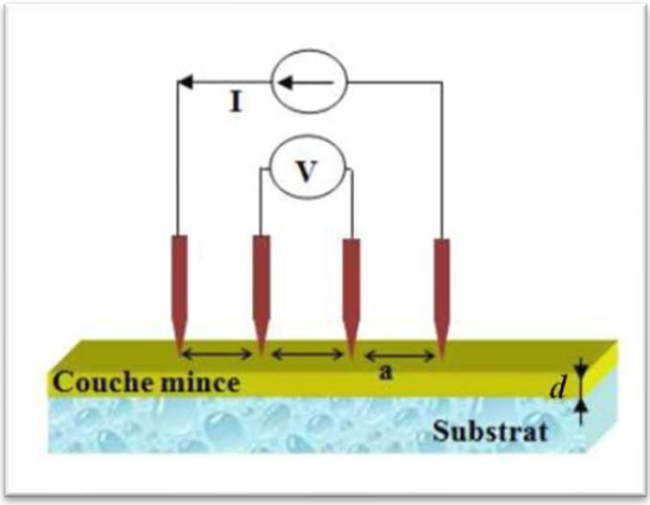


Figure II.18: Diagram representing the principle of the four points method [1,48].

The surface resistance of our samples (R_s) is determined by Ohm's law [1,48]:

$$R_s = \frac{\pi}{ln\,2}\frac{V}{I} \quad \text{(II.5)}$$

Thus, the electrical conductivity of the film (σ) is related to its thickness (d) by the following expression:

$$\sigma = \frac{1}{R_s d} \quad \text{(II.6)}$$

To quantify the electrical conductivity (σ) of samples made, a Jandel RM3-AR multi-position four-point probe was used (Figure II.19). The probe consists of four linearly aligned tungsten carbide tips with an equal distance (a= 1 mm) between each point of contact. Voltage (*V*) and current (*I*) were measured across the inner electrodes by means of a Keithley 2400 source meter, offering high-precision low-voltage measurement. The ratio of (*V*/*I*) was then calculated and averaged for accuracy [1,48].

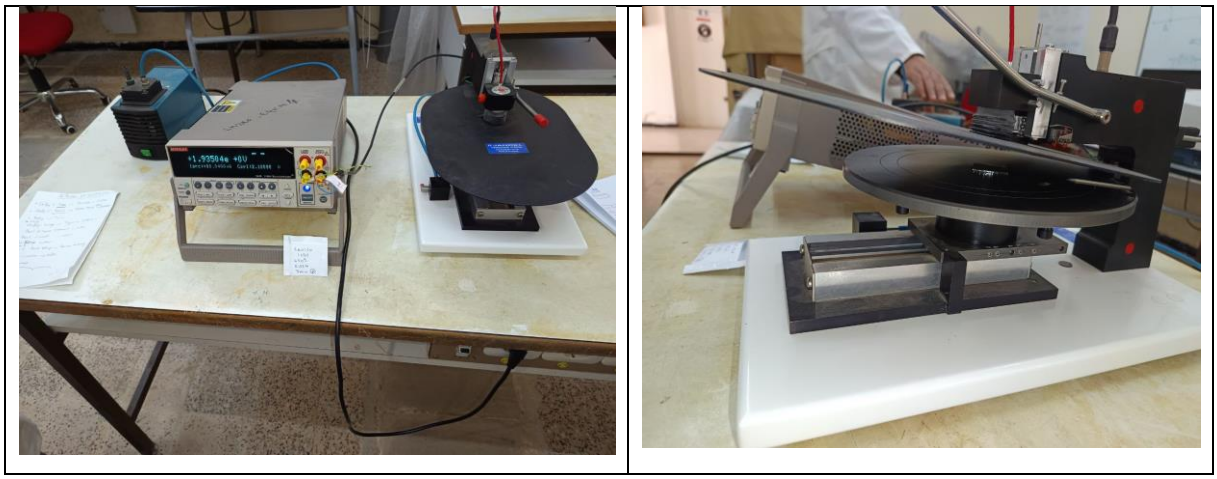


Figure II.19. Jandel RM3-AR Multi-position 4 Point Wafer Probe

Chapter III

Results and discussion



Chapter III: Results and discussion

In this chapter, we present the effect of tin (Sn) doping percentage and the effect of annealing in air (T_s=350 °C and t_R=60 min) on the optical and electrical properties of copper oxide (CuO) thin films doped with different percentages of Sn (0 *at*. %, 3 *at*. %, 6 *at*. %, 9 *at*. %, and 12 *at*. %) deposited under constant conditions (T_S, C, d, φ_s, and t_D) using the ultrasonic spray pyrolysis technique. To study these properties, we will characterize our samples using various analytical techniques such as:

- UV-Visible-NIR spectrophotometry to discuss the optical transmittance spectrum and calculate from this spectrum: the film thickness (d), the refractive index (n), the optical gap energy (Eg), and the Urbach energy (E_{Urb}).
- The four-point technique to measure the electrical conductivity of our samples.

III.1 Photos of the Samples:

Table III.1. Photographs of Cu_xO: Sn thin films deposited onto glass substrates.

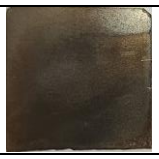
CuO:Sn % *at.*	**0%**	**3%**	**6%**	**9%**	**12%**	**100%**
Before annealing						
After annealing						

Table III.1 shows digital photographs of (Cu_xO: Sn) samples deposited on glass substrates with different Sn atomic percentages (0 *at*. %, 3 *at*. %, 6 *at*. %, 9 *at*. %, 12 *at*. %, and 100 *at*. %) before and after annealing at 350°C for 60 min. It was observed that all the obtained samples showed variations depending on the doping percentage and the annealing process. Before annealing, the films exhibited a light brown color, which became increasingly transparent with higher Sn doping concentration. After annealing, the color of each sample changed to dark brown in decreasing proportions with increasing doping. These colors have been reported by several authors who confirm that the copper oxide structure consists of CuO and/or Cu_2O phases in all deposited samples [17].

III.2. Effect of Sn-doping and annealing on the optical transmittance of CuO samples

Transmittance spectrum is the most significant property of metal oxide films that enables the study of the optical quality like transparency levels and surface roughness [3].

Figures III.1 and III.2 present the optical transmittance spectra as a function of the incident wavelength of photons, in the UV-Visible-NIR region (300-1100 nm), of the samples (substrate + CuxO: Sn) and of the CuxO: Sn thin films, respectively.

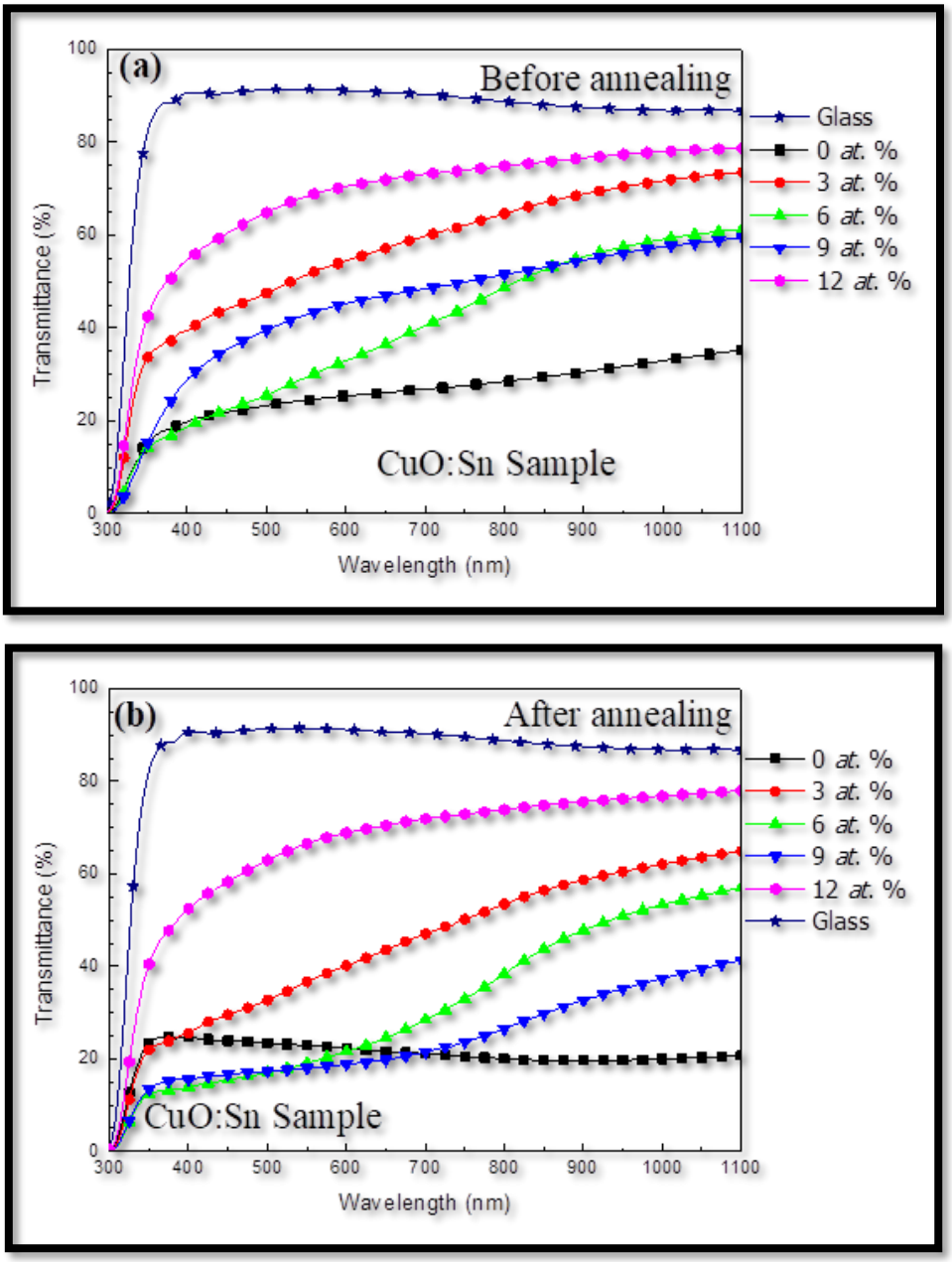


Figure III.1. Variation of optical transmittance of CuO:Sn samples deposited on glass substrates as a function of wavelength for different doping percentages; **(a)**: before annealing, and **(b)**: after annealing.

Which are deposited at 350 °C and 0.05 M by the ultrasonic spray pyrolysis technique at different doping percentages (y=(Sn)/(Sn+Cu) = 0, 3, 6, 9, and 12 *at.* %) before annealing (Figure III.1.a and III.2.a) and after annealing in air at 350°C for 60 min (Figure III.1.b and III.2.b).

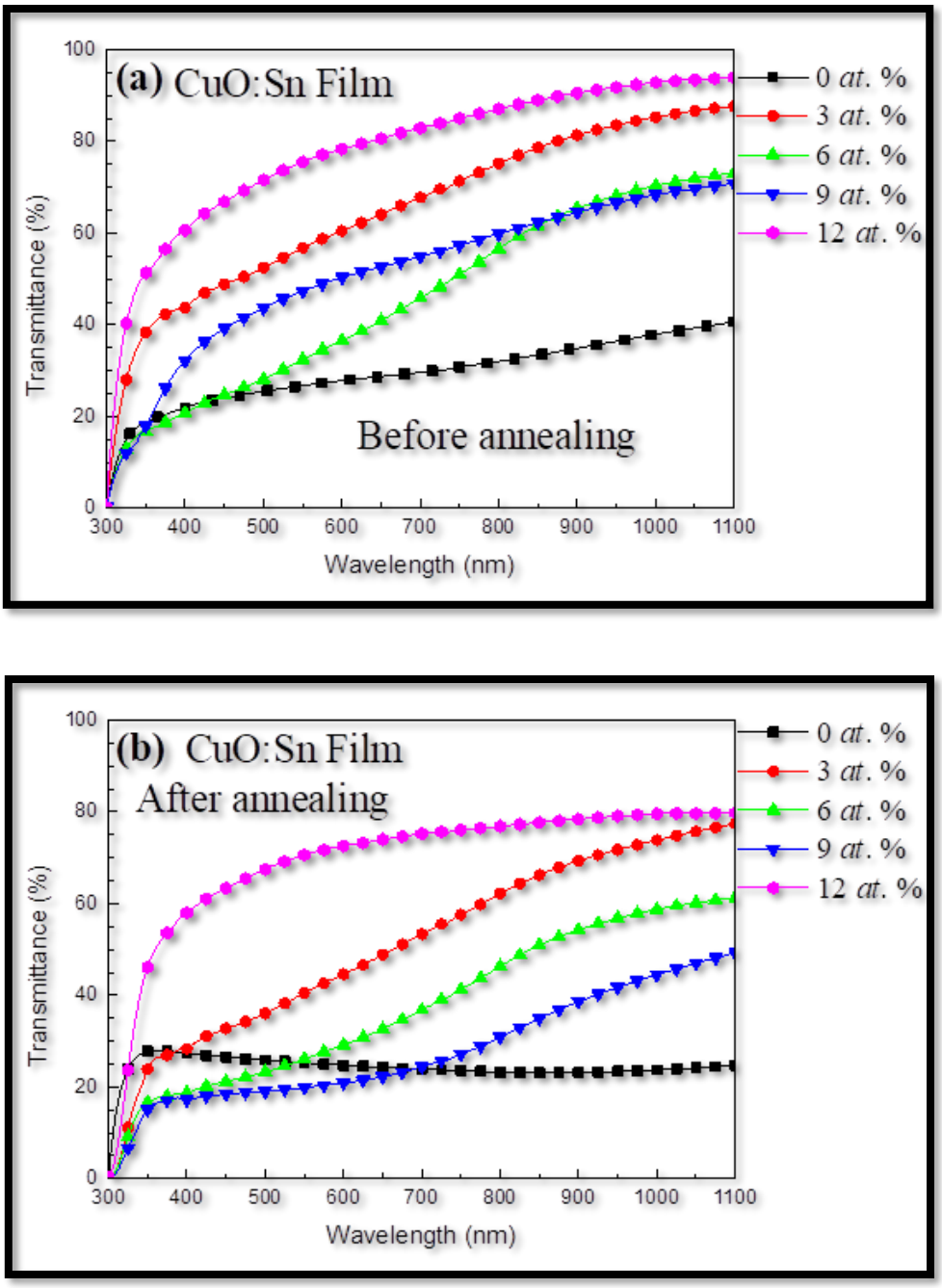


Figure III.2. Variation of optical transmittance of Cu_xO: Sn thin films as a function of wavelength for different Sn concentration values; **(a)**: before annealing, and **(b)**: after annealing.

Figure III.1 (a & b) reveals that the optical transmittance of the samples is influenced by both doping concentration and annealing.

We can observe that the bare glass substrate has high transmittance (T ≈ 90%) in the visible and near-infrared region. On the other hand, the deposited sample show reduced transmittance compared to the glass, suggesting the presence of light absorption by these films.

This is because of the semiconducting nature of CuO, allowing the material to absorb photons in the visible range. This finding has been corroborated by literature, wherein bare glass had an average transmittance of around 91% and lesser transmittance by films that were deposited in a manner similar to ITO and TiO_2 because of inherent light absorption in their crystalline state [53].

Each spectrum exhibits two distinct regions, which are defined by the incident photon wavelength.

The first region for the samples, located between 350 and 1100 nm (Visible and near-infrared domain), the films exhibit low transparency, ranging from 34% to 77% before annealing and 20% to 76% after annealing at λ=1100 nm. These values decrease slightly with the reduction of the wavelength, reaching 15% and 44% before annealing and 14% to 41% after annealing at 350 nm.

In this region, the transmittance of each sample increases slightly with the increase in wavelength. This region is used to determine the thickness of these films and their refractive index [1].

The second region for the samples, with low transmission (absorbing film in the ultraviolet domain) located between 300 and 350 nm, before and after annealing.

This region is used to determine the optical gap energy and the Urbach energy of these layers. Since the incident photons have high energies, the samples exhibit strong absorption and low optical transmittance. This region corresponds to the fundamental absorption in the samples due to inter-band electronic transitions [3].

To determine the optical gap energy of the deposited film (E_g), the Urbach parameter (E_{Urb}), and the type of transition (direct or indirect), the bare substrate is taken as a reference (Figure III.2 (a & b)), and the glass properties are canceled (n_S=1, α_S=0). It can be observed that in the first region of the samples, located between 350 and 1100 nm (in the visible and near-infrared domain), the transmittance varies between 34% and 77% before annealing, and between 20% and 76% after annealing at λ=1100 nm. These values decrease slightly with decreasing wavelength, reaching 15% and 44% before annealing, and between 14% and 41% after

annealing at 350 nm. As for the second region of the films (in the UV domain), it also exhibits low transmittance both before and after annealing.

From (Figure III.2 (a & b)), we observed a increase in optical, transmittance with increasing Sn doping concentration from 0 *at.* % to 12 *at.* %), particularly in the Vis-NIR range (400 – 1100 nm), this occurs due to Sn doping increasing the optical transmittance. This suggests that Sn may reduce copper (Cu) clustering by occupying interstitial sites in the crystal lattice, improving film homogeneity [54]. Higher doping may also alter the bandgap due to Burstein-Moss effect or defect states. and films likely exhibit higher porosity due to incomplete grain growth during deposition [53].

It was observed that the transmittance of these samples is sensitive by annealing. This change is due to the change of the thin films absorption only, not of the glass (Figure III.3).

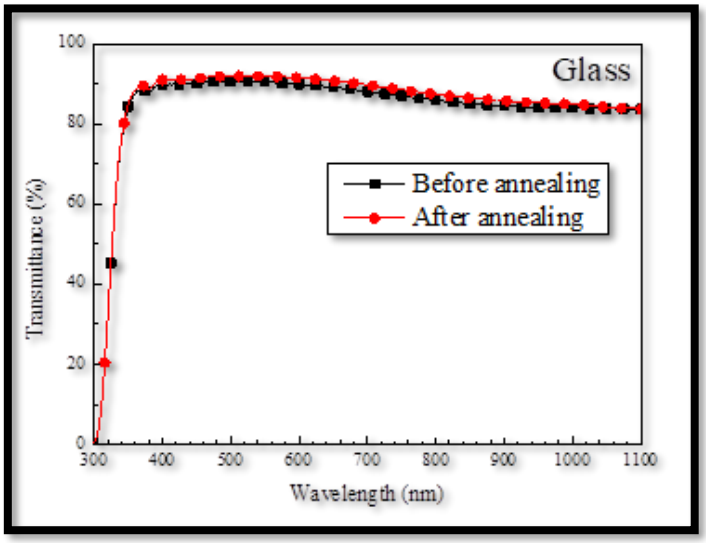


Figure III.3. Variation of optical transmittance of glass as a function of wavelength before and after annealing.

Annealing of Sn-doped CuO thin films makes the optical transmittance decrease. The lowering is a result of the coalescence of grain boundaries, decreasing porosity and densifying the material. Such morphological changes enhance light absorption and scattering and decrease transparency. The findings are consistent with reports on CuO thin films, where high-temperature annealing resulted in grain growth and densification and hence lowering of transmittance [54]. In addition, this decrease may be due to the transformation of the cuprous oxide phase (Cu_2O) to cupric oxide (CuO) by annealing in air at 350°C, which was observed in the color change of the samples from light brown to dark brown (Table III.1).

It was observed that the rate of transmittance decrease gradually diminishes with increasing Sn doping concentration, suggesting that the influence of doping on optical absorption weakens at higher levels (Figure III.4).

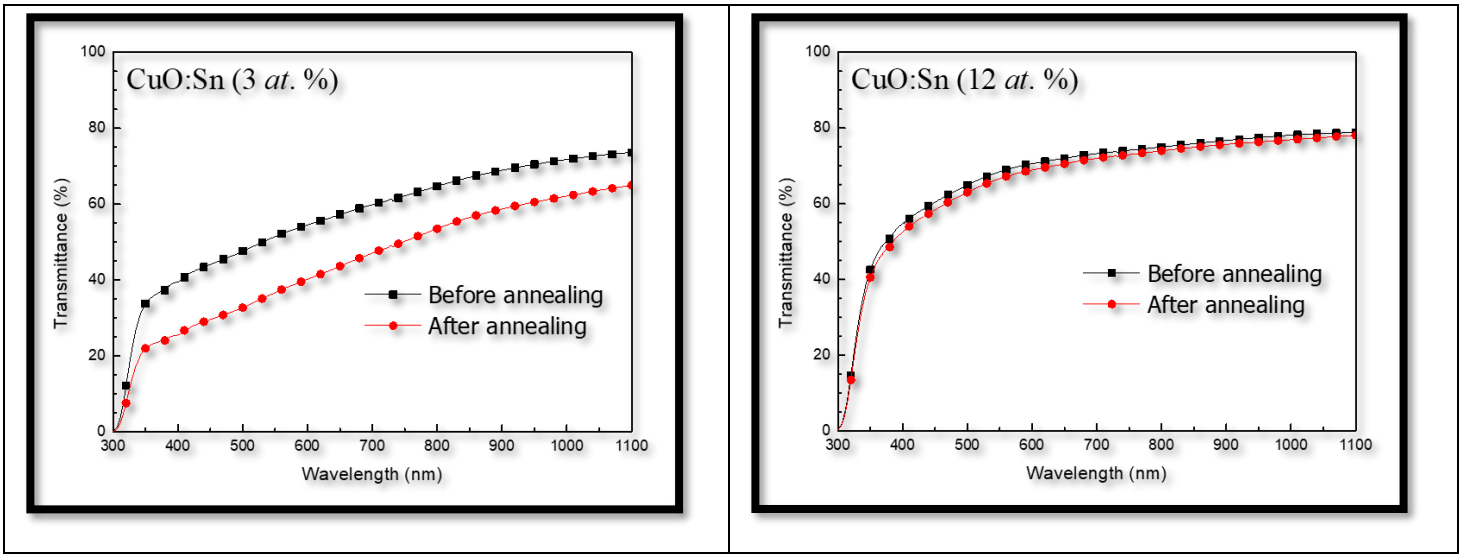


Figure III.4. Variation of optical transmittance of Cu_xO thin films doped by 3 *at*. %, 12 *at*. % of Sn as a function of wavelength before and after annealing.

Due to the fact that SnO_2 is not sensitive to low-temperature annealing (Figure III.5). SnO_2 possesses much higher optical transmittance than CuO primarily due to its higher bandgap (~3.6–4.0 eV) and lower visible absorption. In contrast, CuO with a smaller bandgap (~1.2–1.9 eV) has higher visible absorption and thus lower transparency. This aspect is critical when building optoelectronic devices because the material itself affects light absorption and transmission characteristics [55].

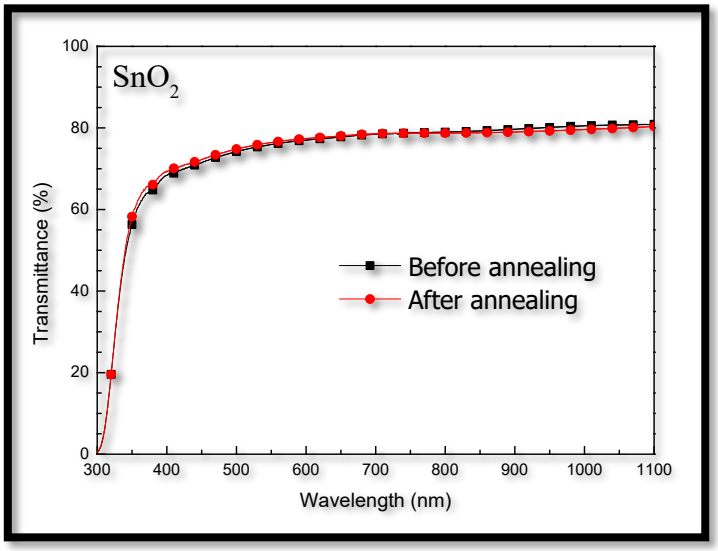


Figure III.5. Variation of optical transmittance of SnO_2 as a function of wavelength before and after annealing.

III.3 Film growth kinetics

III.3.1 The effect of doping and annealing on the thickness of CuO:Sn

We estimated the average thickness of our films from the variation of the optical transmittance according to the wavelength of the incident photon in the UV-Vis-NIR domain using the Swanepoel method which gives highly convergent values which made it possible to deduce a certain number of optical parameters such as: the thickness (d) and the refractive index (n) [56].

Figure III.6 shows the variation of the thickness of CuO:Sn thin films as a function of the doping concentration before and after annealing. It is noted that the thickness values are between 380 and 392 nm before annealing and between 370 and 391 nm after annealing.

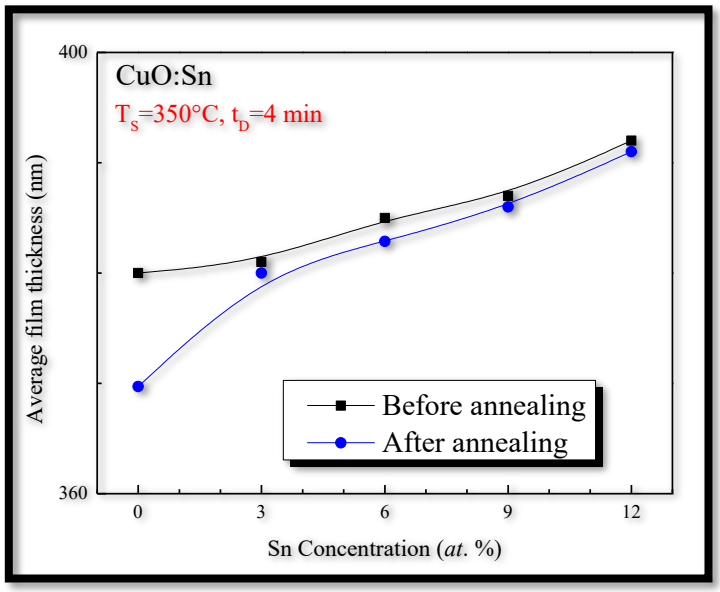


Figure III.6. Variation of the average thickness before and after annealing of CuO:Sn as a function of the different doping percentages.

According to the doping percentage whether before or after annealing, we can see a proportion between increasing of average thickness of copper oxide thin films and increasing in tin concentration (*at*. %). Because the thickness always increases by the increasing of doping even though the type of preparation method and the type of the doper (CuO:Zn, CuO:Ni, ZnO:Ni…) [1,15,17]. The increase of film thickness may be due to the increase in the porosities in the deposited material (CuO:Sn) which makes the material become less density compared to undoped CuO, since it is well known that the variation in thickness is directly proportional to the porosity [4].

By annealing at 350°C in air for 60 min, the thickness of all samples is decreased little, this decrease is due to recrystallization and improvement of the structure of the deposited films which allows to minimize the porosity in the material [3]. Annealing results in an arrangement in the crystal structure and the spaces between atoms become shorter [3].

III.4. Optical characterizations

III.4.1 The effect of doping and annealing on the refractive index of CuO:Sn

The refractive index is a dimensionless parameter which characterizes a medium and defines light propagation in it. Refractive index dispersion is significant in the study of optical materials as well as in optical communications and design of spectral dispersion systems [3]. With Swanepoel's model, the refractive index (n) can be derived by fitting the theoretical transmittance curve onto the experimental spectrum. The method is capable of retrieving critical optical parameters including the film thickness and refractive indices [1,3].

Figure III.7 illustrates the variation of refractive index with the concentration of doping before and after air annealing for CuO:Sn thin films deposited by ultrasonic spray deposition on glass substrates.

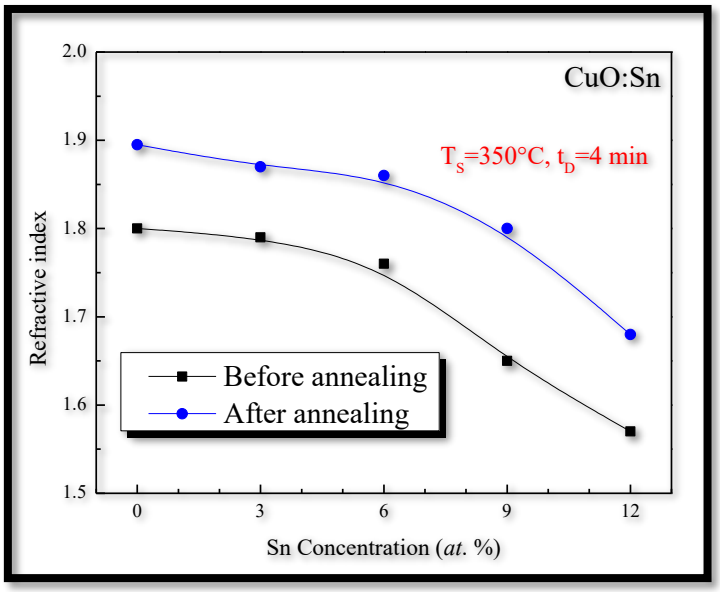


Figure III.7. Variation of the refractive index of thin films before and after annealing of CuO:Sn as a function of doping percentage.

With the increase in Sn concentration in the precursor solution (Sn/(Sn+Cu)) from 0 to 12 *at*. %, the values of the optical refractive index before and after annealing decreased from 1.8 to 1.56 and from 1.89 to 1.67, respectively. This decrease, within this range, can be

attributed to the increase in porosity with the rise in dopant concentration in the deposited films, which have a greater thickness compared to the undoped copper oxide [1,2].

This observation is confirmed by the variation in thickness, as there is an inverse correlation between the change in the refractive index and the thickness (Figure III.8) [1,2].

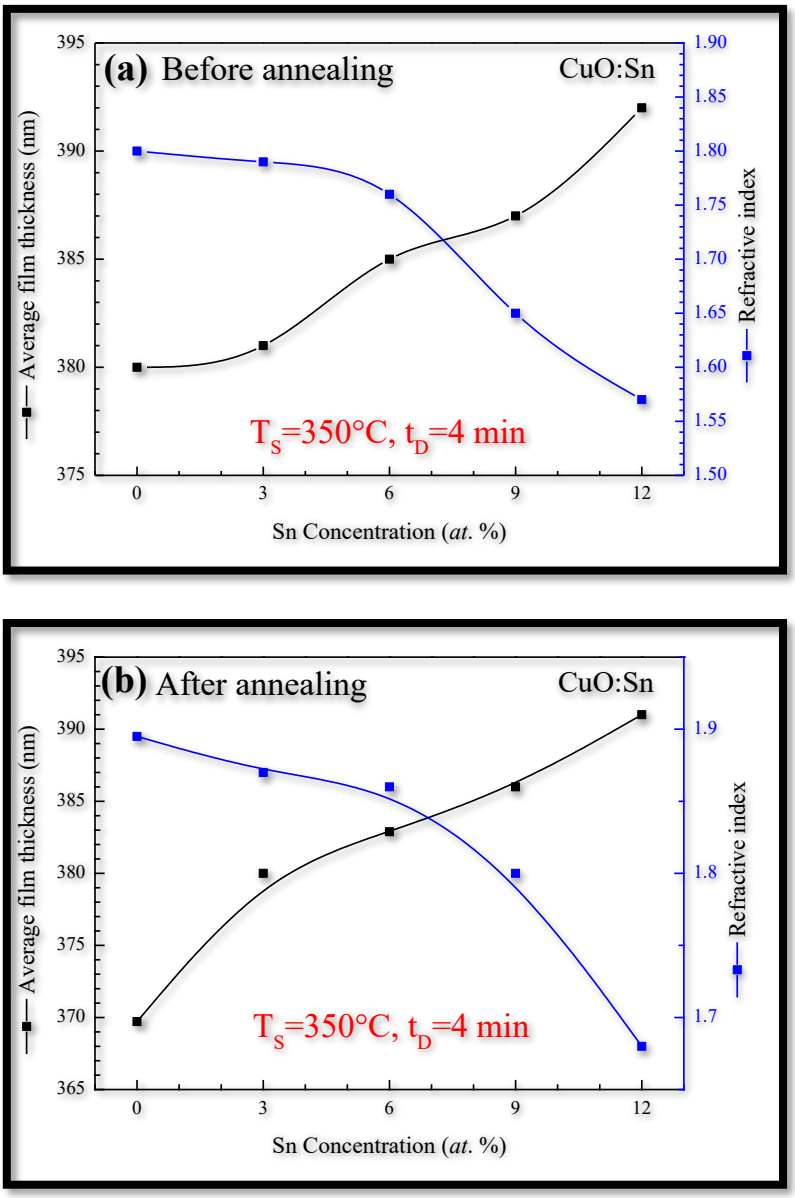


Figure III.8. Variation of thickness and refractive index of thin films before and after annealing of Cu_xO: Sn as a function of doping percentage.

The annealing process enhances the refractive index values due to sample recrystallization. This results in larger grain sizes, decreased porosity, and the material becomes denser [50,57].

III.4.2. The effect of doping and annealing on the Urbach energy of CuO:Sn

Film growth by the spray pyrolysis method occurs through the thermal decomposition of a precipitate on the substrate, resulting from the vaporization of aerosol droplets. In this case, the formed material contains various types of defects, leading to structural disorder [3,17].

From the spectrum of the variation of ln(α) as a function of the photon energy (hυ), all the prepared CuO:Sn samples, both before and after annealing, exhibit a region with a linear dependence on the photon energy. This linear region allows us to determine the Urbach energy (E_{Urb}), which reflects the degree of structural disorder in the thin films resulting from the growth process.

Figure III.9 illustrates the variation of the Urbach energy as a function of Sn concentration for CuO:Sn thin films deposited on glass substrates before and after annealing in air at 350°C.

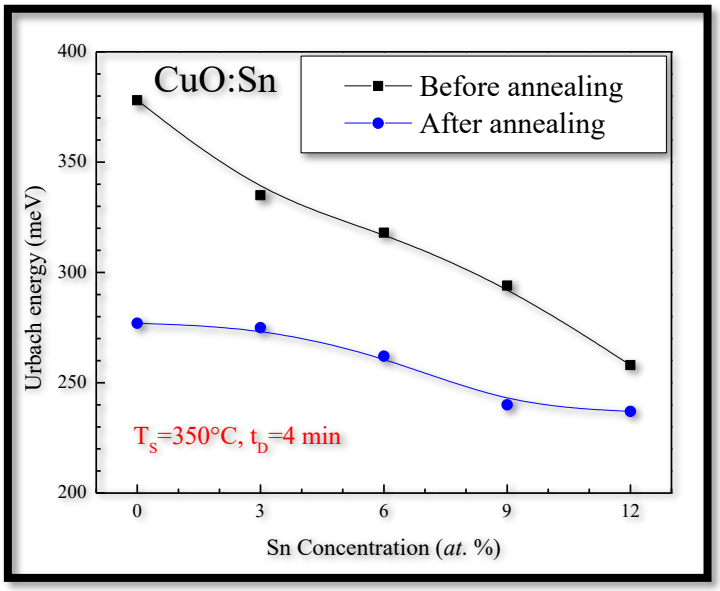


Figure III.9. Variation of the Urbach energy of thin films before and after annealing of CuO:Sn as a function of doping percentage.

Where it is reported that the decrease of Urbach energy (EUrb) with the increase of Sn doping concentration in CuO thin films, and before and after annealing. The trend shows greater structural order with less optical disorder with Sn incorporation [58].

In addition, the Burstein-Moss effect is also able to contribute by shifting the Fermi level and thus suppressing low-energy transitions and eventually broadening the optical bandgap [59,60].

Enhanced optical transparency and reduced carrier scattering in Sn-doped CuO further support the observed decline in Urbach energy [60,61].

Also, since SnO_2 has a good stoichiometry and high transparency compared to CuO (Figure III.10), increasing the concentration of Sn in CuO results in a material with a lower Urbach than CuO.

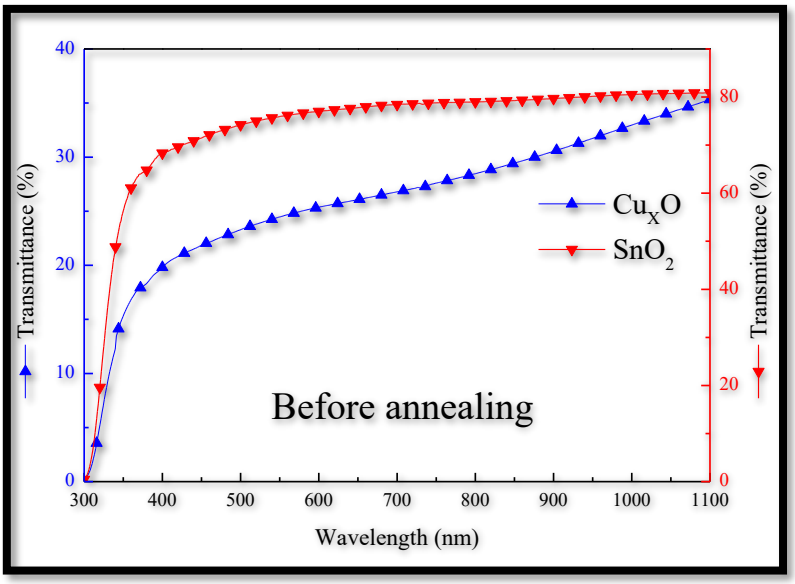


Figure III.10. Variation of optical transmittance of Cu_xO and SnO_2 thin films as a function of wavelength.

By annealing, it is observed that the values of E_{Urb} decrease. This decrease is due to the reduce of defects and impurities by thermal treatment and stoichiometry improves [1]. The decrease in E_{Urb} by annealing can also be interpreted as a result of the reduction in surface porosity and roughness [3].

Indeed, during annealing, the chemical reaction for forming undoped or doped copper oxide becomes more complete due to the grain size growth, and excess elements volatilize, which leads to a material with fewer impurities, minimize disorder and enhance material quality [17].

III.4.3 The effect of doping and annealing on the optical band gap of CuO:Sn

The optical band gaps were estimated from the plots of $(\alpha h\nu)^2$ versus the photon energy (hν) for CuO:Sn thin films deposited by ultrasonic spray pyrolysis technique on glass substrates at different doping levels (0, 3, 6, 9, and 12 *at*. %). Each spectrum exhibits a region that varies linearly with the incident photon energy, indicating that the deposited CuO:Sn has a single optical band gap (Eg) [1]. The value of the optical band gap energy was extracted from the linear region of the spectrum $(\alpha h\nu)^2 = f(h\nu)$ [3].

Figure III.11 shows the variation of optical gap energies (Eg) as a function of doping percentage (*at*.%) of (CuO:Sn) before and after annealing.

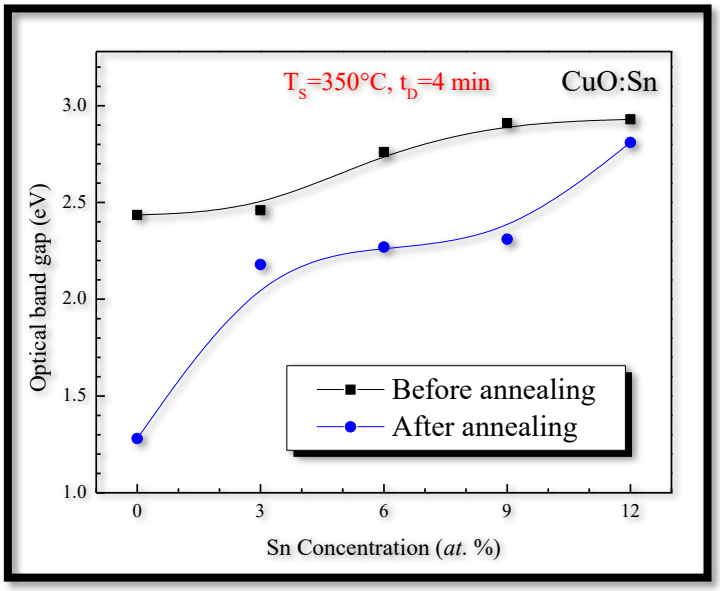


Figure III.11. Variation of the optical gap energy of CuO:Sn thin films before and after annealing as a function of doping percentage.

The Sn-doped CuO thin films optical band gap energy depicts a clear and consistent increase with increasing content of tin (Sn), both before and after annealing. Experimental results show the band gap increases from approximately 2.44 eV to 2.93 eV before annealing, and from 1.28 eV to 2.81 eV after annealing as the Sn content varies from 0 to 12 atomic percent.

This trend agrees with previous reports, which also observed an increase in band gap upon Sn doping. One report, for example, established that the band gap increased from 1.59 eV for pure CuO to 1.75 eV at 12 *wt*.% Sn doping [62].

The band gap widening can be attributed to shifts in the conduction and valence band edges, resulting in a wider optical band gap [63]. Moreover, as SnO_2 has a much higher intrinsic band gap (~3.5 eV), increasing Sn concentration in CuO leads to a composite material with greater band gap characteristics than CuO [62,63].

Through annealing, it is observed that the value of the optical band gap decreases for all samples. This decrease can be interpreted by the increase in grain size of our samples, since grain size always increases with the rise in deposition or thermal treatment temperature, regardless of the fabrication technique used [1,3].

After discussing the optical band gap, it becomes evident that it is closely related to the Urbach energy. As shown in Figure III.12, there is an inverse relationship between them, where the Urbach energy decreases while the optical band gap increases before and after the annealing process [8,52]. This inverse variation reflects the improvement in structural order and the reduction of localized states within the band gap.

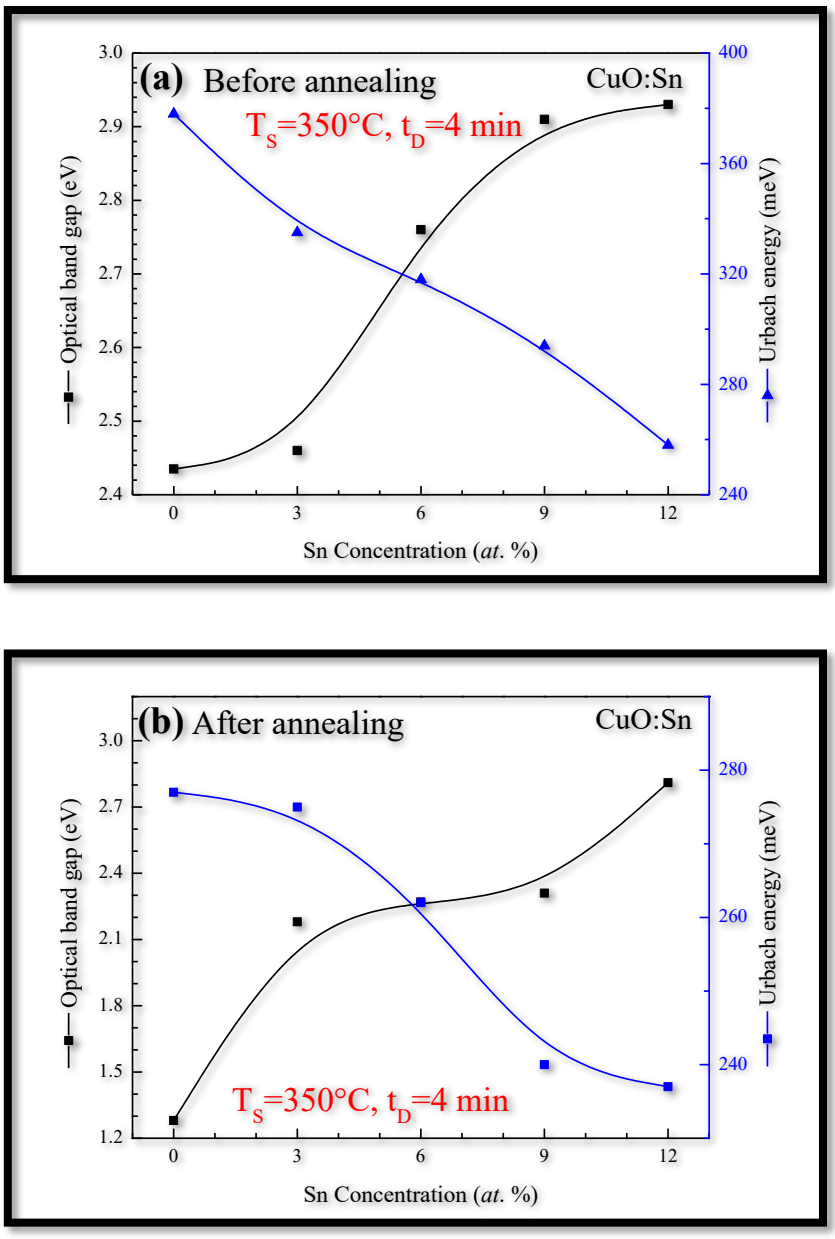


Figure III.12. Variation of the optical band gap and Urbach energy of thin films before and after annealing of Cu_xO:Sn as a function of doping percentage.

III.5. The effect of doping and annealing on the electrical conductivity of CuO:Sn

Metal oxide thin films (for example, SnO_2, CuO, Cu_2O) exhibit superior electrical properties, and thus they are of considerable industrial significance for applications in photovoltaic cells, gas sensors, and lithium-ion batteries. Among these properties, electrical conductivity is a significant parameter [4].

To determine the electrical properties, the four-point probe method is employed, which measures the electrical conductivity [22].

Figure III.13 shows the variation of the electrical conductivity (σ) of the thin films before and after annealing of Cu_xO:Sn as a function of the Sn concentration produced by the ultrasonic spray pyrolysis technique under the same deposition conditions.

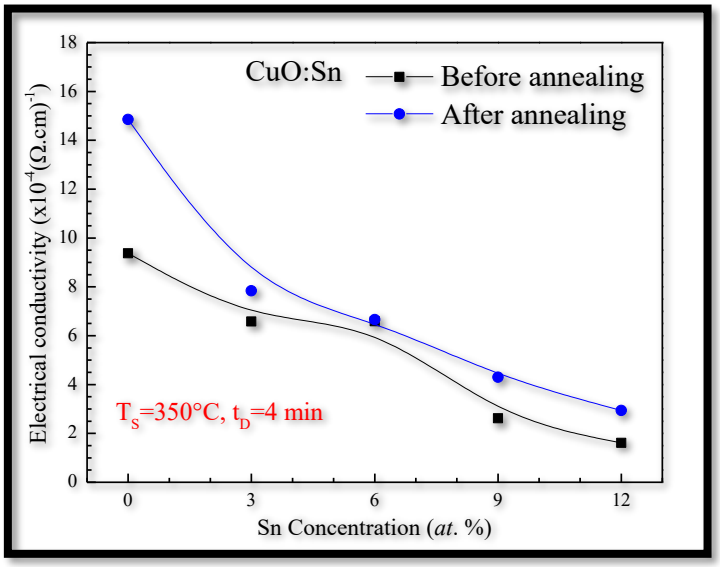


Figure III.13. Variation of electrical conductivity (σ) of Cu_xO:Sn thin films before and after annealing as a function of Sn concentration.

It is seen from this value that the electric conductivity before annealing decreases with concentration of Sn from $9.7x10^{-4}(\Omega.cm)^{-1}$ at 0 *at.* % to $1.9x10^{-4}(\Omega.cm)^{-1}$ at 12 *at.* %.

This decrease in electrical conductivity of Sn-doped CuO thin films with Sn content is attributed to a combination of interconnected mechanisms. The introduction of Sn^{4+} ions replacing Cu^{2+} ions in the CuO lattice decreases the oxygen vacancies, which are otherwise functioning as acceptor species that are responsible for p-type conductivity; this decreases the number of free holes available for conduction [62]. Apart from that, Sn^{4+} also serves as a donor, replacing holes added and thus further decreasing carrier concentration (p) and electrical

conductivity (σ) [62,64]. Reduction of crystallite size and an increase in the density of grain boundaries due to Sn doping result in a loss of available charge states, limiting pathways for charge carriers and reducing overall conductivity (Equation III.1) [64].

$$\sigma = pq\mu_p \quad \text{(III.1)}$$

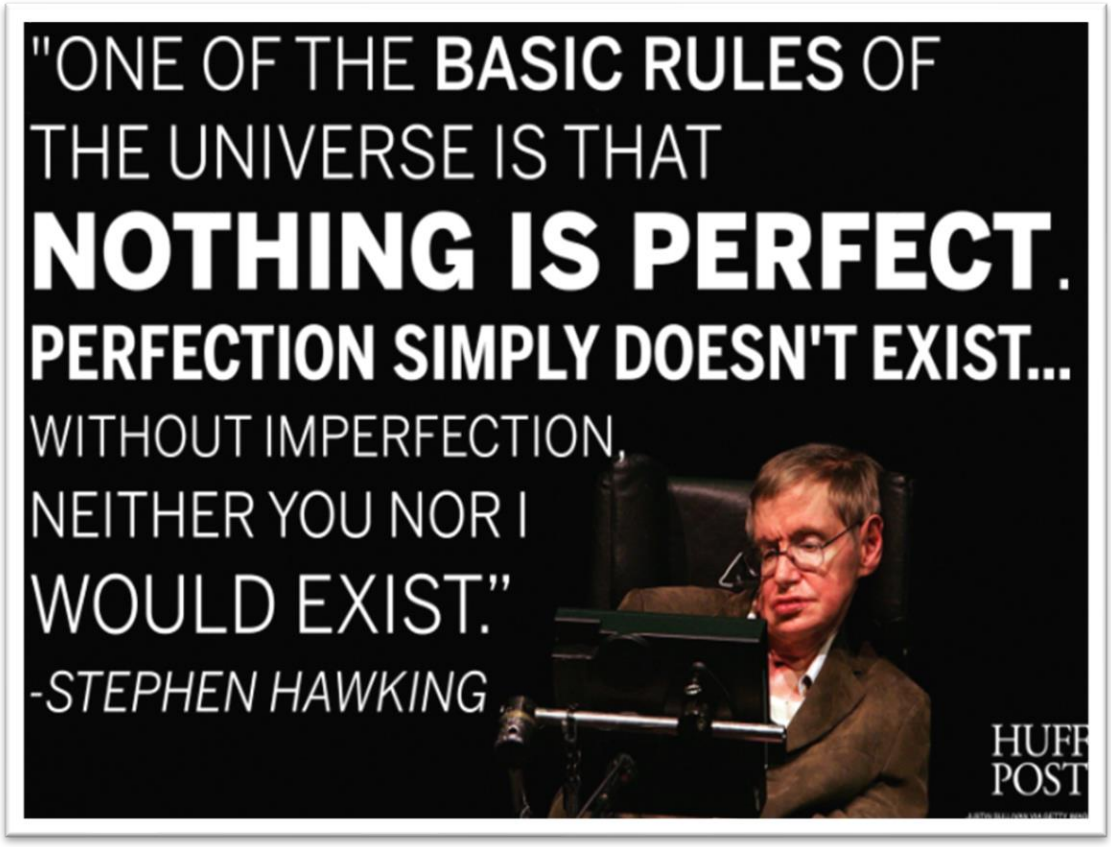
where q and μ_p are the electronic charge and the mobility of charge carriers, respectively.

The electrical conductivity (σ) of Cu_xO:Sn films increase by annealing at 350°C and the highest increase which is from $9.7x10^{-4}(\Omega.cm)^{-1}$ to $1.5x10^{-3}(\Omega.cm)^{-1}$ for undoped copper oxide. This may be due to the excess oxygen content in the copper oxide. Drobny and Pulfrey reported that during the transition from Cu_2O to CuO. The electrical conductivity increases by annealing due to the formation of the tenorite phase [17].

$$2Cu_2O + O_2 \longrightarrow 4CuO \quad \text{(III.2)}$$

An increase of the conductivity at this phase might be caused by an increase in the charge carriers density (Equation III.1) [17].

Conclusion


"ONE OF THE BASIC RULES OF
THE UNIVERSE IS THAT
NOTHING IS PERFECT.
PERFECTION SIMPLY DOESN'T EXIST...
WITHOUT IMPERFECTION,
NEITHER YOU NOR I
WOULD EXIST."
-STEPHEN HAWKING
HUFF
POST

General conclusion

Research work conducted in this thesis deals with the study of the effect of tin doping and annealing on copper oxide thin films properties produced through the ultrasonic spray pyrolysis technique. CuO:Sn doped thin films were deposited on glass substrates for different doping amounts (0, 3, 6, 9, and 12 *at*. %) from an aqueous solution of copper (II) chloride dihydrate and tin (II) chloride dihydrate. The substrate temperature, nozzle-substrate distance, spray rate, and spray time were kept constant throughout the deposition process at 350 °C, 5 cm, 60 ml/h, and 4 min, respectively. After preparation, the samples were characterized by UV-Visible spectrophotometry, and the four-point probe method to determine their optical and electrical properties. These samples were also characterized after annealing in air at 350 °C for 60 minutes.

According to this study, all the samples before annealing appeared light brown in color, becoming increasingly transparent as the Sn concentration increased. After annealing, each sample turned dark brown, with the color intensity decreasing as the Sn doping increased.

The characterization led to the following conclusions:

- With increased Sn doping, the average thickness, optical transmittance and optical band gap of the samples increased, while the refractive index, Urbach energy, and electrical conductivity decreased. These variations are interpreted as resulting from substitution of Cu^{2-} ions with Sn^{4+} in the CuO lattice, increased porosity, and decreased both the concentration and mobility of charge carriers.
- The annealing effect led to a decrease in average thickness, Urbach energy, and optical band gap, optical transmittance, along with an increase in refractive index, and electrical conductivity. These changes are explained by recrystallization of the samples and purification of the deposited layer structure, reducing porosity and impurities and increasing grain size and charge carrier concentration in the denser deposited material.
- Finally, CuO:Sn thin films can be said to be good semiconductors for applications such as solar cells, gas sensors, catalysts, electrochromic films, fuel cells, and OLED anodes due to their superior stability, stoichiometry, electrical conductivity, transparency, and adhesion to the substrate compared to undoped copper oxide.

References

References

[1] S. Guellati, C. Boussaha, Étude de l'effet de dopage par nickel et du recuit sur les propriétés des couches minces d'oxyde de cuivre, Master's Thesis, Echahid Cheikh Larbi Tebessi university-Tebessa (2019).

[2] R. Benmerad, Effect of Cr doping on optical and electrical properties of ZnO thin films deposited by spray pyrolysis technique, Master's Thesis, Echahid Cheikh Larbi Tebessi university-Tebessa (2023).

[3] F-Z. Ababsia, S. Fares, Élaboration et caractérisation des couches minces d'oxyde de nickel dopé au cuivre, Master's Thesis, Echahid Cheikh Larbi Tebessi university-Tebessa (2018).

[4] W. Lemouchi, Effect of Cu doping on optical and electrical properties of ZnO thin films deposited by spray pyrolysis technique, Master's Thesis, Echahid Cheikh Larbi Tebessi University-Tebessa (2023).

[5] D. Rahal & T. Zerfaoui, Elaboration of tin dioxide thin films by spray pyrolysis using different concentrations of solution and solvent, Master's Thesis, Echahid Cheikh Larbi Tebessi university-Tebessa (2022).

[6] S. Redjel & N. Mekhaznia, Elaboration and characterization of tin oxide thin films deposited by spray pyrolysis, Master's Thesis, Echahid Cheikh Larbi Tebessi university-Tebessa (2020).

[7] M. Mozafarifard, D. Toghraie, Numerical simulation of fractional non-fourrier heattransfert metal films under short-pluse laser, Ineternational communaications in heat and mass transfert 115 (2020) 1-9.

[8] K. Khlaifia, Structural and opto-electrical stydy of SnO2 thin films elaborated by spray pyrolysis, Master thesis, Hamma Lakhder university-El-oued (2015).

[9] O. Belahssen, Elaboration and characterization of thin-film gas sensor, Echahid Hamma Lakhdar University- El-Oued (2019).

References

[10] J.B.Chaudhari, Growth and study of optical and electrical properties of chemically deposited CdS1-xSex:Ag nano composite thin films for sensor application, Doctorat Thesis, University of Rajasthan, Jaipur- India (2014).

[11] K. Bennaceur, Elaboration and characterization of SnO_2:In thin films deposited by spray pyrolysis technique, Doctorate's Thesis, Mohamed Kheider University-Biskra (2020).

[12] C. Khelifi, Tin dioxide SnO_2 thin films deposited by ultrasonic spray technique:Properties and Applications, Doctorate's Thesis, Mohamed Kheider University-Biskra (2018).

[13] O. Daranfad, Elaboration et caractérisation des couches minces de Sulfure de Zinc préparées par spray ultrasonique, Magister's Thesis, Mentouri University- Constantine (2013).

[14] P. A. Savale, Physical vapor deposition (PVD) methods for synthesis of thin films: A comparative study, Archives of Applied Science Research 8, (2016) 1–8.

[15] M. Messaouda, Influence du recuit sur les propriétés optoélectroniques des couches minces de $(ZnO)_{1-x}(NiO)_x$, Master's Thesis, Echahid Cheikh Larbi Tebessi University-Tebessa (2015).

[16] A. Jilani, M. Shaaban, A.H. Hammad, Ch. 8: Advance deposition techniques for thin film and coating, Intech Open (2017) 137-149.

[17] N. Menasraia & H. Talbi, Élaboration et caractérisation de couches minces d'oxyde de cuivre dopé par zinc, Master' s Thesis, Echahid Cheikh Larbi Tebessi University-Tebessa (2017).

[18] S. Kemach, Élaboration et caractérisation de couches minces de Ni1-xZnxO, Master' s Thesis, Echahid Cheikh Larbi Tebessi University-Tebessa (2014).

[19] A. Jilani, M. Shaaban, A.H. Hammad, Advance deposition techniques for thin film and c oating, IntechOpen 33 (2017) 138-147.

[20] A. Hannachi, A. Segura, H.M. Meherzi, Growth of manganese sulfide (α-MnS) thin films by thermal vacuum evaporation: Structural, morphological, optical properties, Materials Chemistry and Physics 6 (2016) 326–332.

References

[21] G-K. Wolf, K. Zucholi, M. Barth, and W. Ensinger, Equipment for ion beam assisted deposition, Nucl. Instruments Methods Phys. Res. Sect. B Beam Interact. with Mater. Atoms 21, (1987) 570–573.

[22] B. Maatoub & S. Fissah, Study of the optical and Electrical properties of tin oxide thin films deposited by spray pyrolysis technique, Master's Thesis, Echahid Cheikh Larbi Tebessi University-Tebessa (2021).

[23] A. Hafdallah, Étude du dopage des couches minces de ZnO élaborées par spray ultrasonique, Magister's Thesis, Mentouri University- Constantine (2007).

[24] A. Jilani, M. Shaaban, A.H. Hammad, Advance deposition techniques for thin film and coating, IntechOpen 33 (2017) 138-147.

[25] F. Bouaichi, Deposition and analysis of Zinc Oxide thin films elaborated using spray pyrolysis for photovoltaic applications, Doctorate's Thesis, Mohamed Kheider University-Biskra (2019).

[26] R. Dorey, Routes to thick films: What is a thick film? How isitmade?, Ceramic Thick Films for MEMS and Microdevices, Ch. 2 (2012) 35-61.

[27] S. Eränen, A. Inoue, In Handbook of silicon based MEMS materials and technologies (Second Edition), Emerging Nanotechnologies for Manufacturing A volume in Micro and Nano Technologies Book, 2nd edition (2015) 79‑159.

[28] J. E. Mellor and Accepted, Investigation of a Sol-Gel Coating Technique for Polarized 3 He Target Cells, College of William and Mary in Virginia, (2001).

[29] K. Bedi, S. MISHRA Alcohol sensing of tin oxide thin film prepared by sol–gel process, thin Film., 25 (2002) 231–234.

[30] R. S. Sonawane, S. G. Hegde, and M. K. Dongare, Preparation of titanium (IV) oxide thinfilm photocatalyst by sol-gel dip coating, Mater. Chem. Phys 77, 3, (2003) 744–750.

[31] G. Diego, J. Rodriguez, Frequency-domain circuit analysis, Material sience and materials engineering, Ch.1 (2019)16-30.

[32] H. Lekiket, Élaboration et caractérisation des films ZnS par bain chimique, Ph.D. dissertation, Univ. Frères Mentouri-Constantine (2016).

References

[33] I. Amroune, B. Bendjedji, Effet de la température de dépôt du système CuO–Cu_2O par spray chimique, Master's thesis, Mohamed Boudiaf University-M'Sila (2018).

[34] H. MOUALKIA, Elaboration et Caractérisation de Couches Minces de Sulfure de Cadmium (CdS), Doctorate's Thesis, Universite Mentouri-Constantine (2010).

[35] A. Belaoura, Étude de l'effet dedopage par Sn sur les propriétés des couches minces deZnO, Master's Thesis, Echahid Cheikh Larbi Tebessi University-Tebessa (2016).

[36] A. Hannachi, A. Segura, H.M. Meherzi, Growth of manganese sulfide (α-MnS) thin films by thermal vacuum evaporation: Structural, morphological, optical properties, Materials Chemistry and Physics 6 (2016) 326-332.

[37] A. Sari & S. Bouchrit, Elaboration et caractérisation des couches minces d' oxyde de cuivre non dopé, Master' s Thesis, Echahid Cheikh Larbi Tebessi University-Tebessa (2017).

[38] W. Menesklou, H. Schereiner, K. Hardtl & E. Ivers, High temperature oxygen based ondoped SrTiO3, Sensors and Actuators B 59 (1999) 184-189.

[39] L. Herissi, Élaboration et caractérisation de couches minces d'oxydes métalliques destinées à des applications optoélectroniques, Doctorate's Thesis, Larbi Ben M'hidi University-Oum El Bouaghi (2016).

[40] H. Ben Yessaad, N. Sehili, Électrodéposition et caractérisation des couches minces d'oxyde cuivrique CuO, Master's Thesis, Mohamed El Bachir El Ibrahimi University-Bordj Bou Arreridj (2017).

[41] S. Mehadjebi, La synthèse des nano poudres de CuO avec la méthode précipitation Sol-Gel en utilisant le précurseur $CuSO_4$ et l'étude de leurs propriétés structurales et optiques, Master's thesis, Mentouri University - Constantine (2015).

[42] A-A. Ogwu, E. Bouquerel, O. Ademosu, S. Moh, E. Crossan, F. Placido, ActaMaterialia, 53 (2005) 5151.

References

[43] D. Perednis and L. J. Gauckler, Thin Film Deposition Using Spray Pyrolysis, Electroceramics, 14, (2005)103–111.

[44] G. M. Stoian, physical properties of magnetic as grown and oxygen annealed SnO2: CO thin films, Florida State University (2013).

[45] M. Farida, Préparation et caractérisation de couches minces d'oxyde de titane (TiO_2) etdu couple d'oxydes (TiO_2/SnO_2), Master's thesis, Universite Mentouri-Constantine (2012).

[46] M. Selma. H.A. Fadheela, H. Oleiwe, J.H. Khulaef, Preparation and characterization oftin oxide thin films by using spray pyrolysis technique, Tech Journal 33 (2015) 529-538.

[47] H-K. Mobarka, N. Haddar, L'influence du temps de dépôts sur les propriétés des couches minces de CuO élaborées par spray pneumatique, Master's thesis, Mohamed Khider University-Biskra (2020).

[48] W. Boutaghout, A. Guechi, Structural, optical and electrical properties of (AZO/CuO/ZnO and AZO/CuO/SnO_2) heterostructures prepared by spray pyrolysis intended for the photodetection of ultraviolet light, Master's Thesis, Larbi Ben M'hidi University, Oum El Bouaghi, (2022).

[49] F. Kermiche, Elaboration de couches minces ZnO par ablation laser et caractérisation physique, doctorate's thesis, Mentouri University-Constantine (2015).

[50] C. S. Wiliams, O. Becklund, Optics: A Short Course for Engineers and Scientists, John Wiley et sons, (1972).

[51] T. Gungor, H. Tolunay, Drift mobility measurements in a-SiNx:H, Journal of Non- Crystalline Solids 282, (2001) 197-202.

[52] Natsume Y, Sakata H, Hirayama T, Low temperature electrical conductivity and optical absorption edge of ZnO films prepared by chemical vapor deposition, Phys Stat Sol (A) 148, (1995) 485–95.

[53] A. K. Jha et al., Influence of oxygen vacancies and dopants on the optical and structural properties of CuO thin films, Applied Surface Science 499, (2020)143945.

References

[54] S. Kumar, M. K. Yadav, and S. C. Jun, Effects of Sn doping on the structural, optical, and electrical properties of CuO thin films, Journal of Alloys and Compounds 741, (2018) 648–656.

[55] N. F. Habubi, S. F. Oboudi, and S. S. Chiad, Study of Some Optical Properties of Mixed SnO_2-CuO Thin Films, Journal of Nano- and Electronic Physics 4, 4, (2012) 04008-1–04008-4.

[56] R. Swanepoel, Determination of the thickness and optical constants of amorphous silicon, Journal of Physics E: Scientific Instruments 16 (1983) 1214.

[57] I. Djebri, Élaboration et caractérisation des couches minces de CuO dopé Y, Master's Thesis, Echahid Cheikh Larbi Tebessi University-Tebessa (2023).

[58] S. Nagabhirava, A. N. Fiore, L. Tang, and P. R. Nair, Unveiling the nature of room-temperature-fabricated p-type SnO thin films: the critical role of intermediate phases, lattice disorder, and oxygen interstitials, Materials Advances 5, 1, (2024) 350–361.

[59] Md. Kamruzzaman, M. H. Nishat, Md. Mintu Ali, M. Humayan Kabir, and M. S. Rahman, Influence of multi-doping (Zn and Sn) on the optical, and electrical properties of spray-deposited CdO thin films, Physica B: Condensed Matter 690, (2024).

[60] S. Mahjoub, M. Mezeyeh, G. El Fidh, N. Bitti, and E. Llobet, The influence of Sn particle incorporation on the photocatalytic activity of sprayed ZnO–SnO nanocomposites, Scientific Reports 12, 1, (2022) 1–12.

[61] H. D. Abdullah, H. F. Al-Taay, M. K. Khalaf, H. F. Oleiwi, and A. J. Rahma, "Structure, Morphology and Optical Properties of SnO_2 Nanoparticle Synthesized via Ultrasonic Spray Pyrolysis Technique: Effect of CuO Doping Concentration," in J. Phys.: Conf. Ser, 2114, 012074, (2021).

[62] P. Venkateswari, P. Thirunavukkarasu, T. Sivakumar, and G. Sankar, Characterization of Pure CuO and Sn Doped CuO Thin Films Via JNSP Technique for P-N Junction Diode Application, IOSR Journal of Engineering (IOSRJEN) 9, (2019) 51–60.

References

[63] A. S. M. Arifin, M. A. Mahmud, A. M. M. Taufique, and M. A. Hakim, Influence of Sn doping on CuO thin films for optoelectronic applications, Manipal Research Colloquium (MRC).

[64] Naoual Al Armouzi, Mohamed Manoua, Hikmat S. Hilal, Ahmed Liba, and Mustapha Mabrouki, Multi-Layered Sol–Gel Spin-Coated CuO Nanofilm Characteristic Enhancement by Sn Doping Concentration, Processes 11, (2023)1– 15.

Effect of Sn doping on optical and electrical properties of CuO thin films deposited by spray pyrolysis technique

Abstract

The aim of this work is the study of the effect of tin (Sn) doping and annealing on the optical and electrical properties of copper oxide (CuO) thin films deposited by ultrasonic spray pyrolysis technique to obtain good photoelectric properties it an important candidate in many technological applications.

In this work, we have prepared these films onto glass substrates with different Sn concentrations from 0 to 12 at. % in the aqueous solution of copper (II) chloride dihydrate and tin (II) chloride dihydrate as precursors. Substrate temperature, solution concentration, nozzle-substrate distance, and the deposition time were kept constant during the whole deposition process.

These films were characterized, before and after annealing, using the UV-Visible-NIR Spectrophotometer and the four-point method to determine their optical and electrical properties. All samples obtained have good physical properties that varied with the doping percentage and the annealing.

It should be noted that increasing Sn doping in CuO films leads to an increase in thickness and optical band gap, while the refractive index, optical transmittance, Urbach energy, and electrical conductivity decrease. On the other hand, annealing reduces the thickness, band gap, Urbach energy, and optical transmittance, while increasing the refractive index and electrical conductivity.

Keywords: Cu_xO:Sn thin films, Spray pyrolysis, Annealing, Optical transmission, Optical band gap, Electrical Conductivity.

Effet du dopage par Sn sur les propriétés optiques et électriques des couches minces de CuO déposées par la technique de spray pyrolyse

Résumé

L'objectif de ce travail est l'étude de l'effet du dopage par l'étain (Sn) et le recuit sur les propriétés optiques et électriques des couches minces d'oxyde de cuivre (CuO) déposées par la technique de spray pyrolyse ultrasonique, afin d'obtenir de bonnes propriétés photoélectriques, ce qui en fait un candidat prometteur dans de nombreuses applications technologiques.

Dans ce travail, nous avons préparé ces films sur des substrats en verre avec différentes concentrations d'étain allant de 0 à 12 % *at*. dans une solution aqueuse contenant du chlorure de cuivre (II) dihydraté et du chlorure d'étain (II) dihydraté comme précurseurs. La température du substrat, la concentration de la solution, la distance bec-substrat ainsi que le temps de pulvérisation ont été maintenus constants tout au long du processus de dépôt.

Ces échantillons ont été caractérisés avant et après recuit à l'aide d'un spectrophotomètre UV-Visible-NIR et de la méthode des quatre pointes pour déterminer leurs propriétés optiques et électriques.

Tous les échantillons obtenus présentent de bonnes propriétés physiques qui varient en fonction du pourcentage de dopage par Sn et par le recuit.

Il convient de noter que l'augmentation de dopage par Sn dans les films de CuO entraîne une augmentation de l'épaisseur et du gap optique, tandis que l'indice de réfraction, la transmittance optique, l'énergie d'Urbach et la conductivité électrique diminuent. En revanche, le recuit provoque une réduction de l'épaisseur, du gap optique, de l'énergie d'Urbach et de la transmittance, accompagnée d'une augmentation de l'indice de réfraction et de la conductivité électrique.

Mots-clés: Couches minces de Cu_xO:Sn, Spray pyrolyse, Recuit, Transmission optique, Gap optique, Conductivité électrique.

ملخـــص

تأثير التطعيم بالقصدير على الخصائص البصرية والكهربائية للأغشية الرقيقة لأكسيد النحاس المحضرة بتقنية الرش بالانحلال الحراري

ملخـــص

يهدف هذا العمل إلى دراسة تأثير التطعيم بالقصدير (Sn) والتلدين على الخواص الضوئية والكهربائية للأغشية الرقيقة لأكسيد النحاس (CuO) المترسبة باستخدام تقنية الرش بالانحلال الحراري بواسطة الأمواج فوق الصوتية، وذلك للحصول على خصائص كهروضوئية جيدة، مما يجعلها مرشحًا واعدًا للعديد من التطبيقات التكنولوجية.

في هذا العمل، قمنا بترسيب هذه الأغشية على ركائز زجاجية وفق نسب مئوية ذرية مختلفة من القصدير (من 0 إلى 12%) في محلول مائي يحتوي على ثنائي كلوريد النحاس ثنائي الهيدرات وثنائي كلوريد القصدير ثنائي الهيدرات كمواد أولية. تم الحفاظ على ثبات كل من درجة حرارة الركيزة، تركيز المحلول، المسافة بين الفوهة و الركيزة ، وزمن الرش خلال عملية الترسيب .

تم توصيف هذه العينات قبل وبعد التلدين، باستعمال جهاز المطياف الضوئي للأشعة فوق البنفسجية – المرئية – وتحت الحمراء القريبة باللإضافة إلى طريقة المسابير الأربعة لتحديد خصائصها الضوئية والكهربائية.

أظهرت جميع العينات المتحصل عليها خصائص فيزيائية جيدة تختلف باختلاف نسبة التطعيم بالقصدير والتلدين. وقد لوحظ أن زيادة نسبة القصدير في أفلام أكسيد النحاس تؤدي إلى زيادة السمك و فجوة النطاق الضوئي، بينما تنخفض كل من قرينة الانكسار، النفاذية الضوئية، طاقة أورباخ والناقلية الكهربائية. من ناحية أخرى، يُقلل التلدين كل من السُمك، وفجوة النطاق الضوئي، طاقة أورباخ والنفاذية الضوئية، مع زيادة معامل الانكسار والتوصيل الكهربائي.

الكلمات المفتاحية: الشرائح الرقيقة من $Cu_xO:Sn$، الرش بالانحلال الحراري، التلدين، النفاذية الضوئية، فجوة النطاق الضوئي، الناقلية الكهربائية.